

## RESEARCH PAPER

# Discovery of a novel, potent and selective small-molecule inhibitor of PD-1/PD-L1 interaction with robust *in vivo* anti-tumour efficacy

Chenglong Liu<sup>1</sup> | Feilong Zhou<sup>2</sup> | Ziqin Yan<sup>2</sup> | Lian Shen<sup>1</sup> | Xichen Zhang<sup>2,3</sup> | Fenglian He<sup>1</sup> | Heng Wang<sup>1</sup> | Xiaojie Lu<sup>2</sup> | Ker Yu<sup>1</sup> | Yujun Zhao<sup>2,3,4</sup> | Di Zhu<sup>1,5</sup>

<sup>1</sup>Department of Pharmacology, School of Pharmacy, Fudan University, Shanghai, China

<sup>2</sup>State Key Laboratory of Drug Research, Shanghai Institute of Materia Medica, Chinese Academy of Sciences, Shanghai, China

<sup>3</sup>School of Pharmacy, University of Chinese Academy of Sciences, Beijing, China

<sup>4</sup>School of Pharmaceutical Sciences, Zhengzhou University, Zhengzhou, China

<sup>5</sup>Key Laboratory of Smart Drug Delivery and Shanghai Engineering Research Center of Immune Therapy, Fudan University, Shanghai, China

## Correspondence

Yujun Zhao, State Key Laboratory of Drug Research, Shanghai Institute of Materia Medica, Chinese Academy of Sciences, Shanghai 201203, China.  
Email: yjzhao@simm.ac.cn

Di Zhu, Department of Pharmacology, School of Pharmacy, Fudan University, Shanghai 201203, China.  
Email: zhudi@fudan.edu.cn

## Funding information

Science and Technology Commission of Shanghai Municipality, Grant/Award Number: 18431907100; National Science & Technology Major Project “Key New Drug Creation and Manufacturing Program”, China, Grant/Award Numbers: 2018ZX09711002-005, 2018ZX09711002-004-010; Shanghai Science and Technology Commission, Grant/Award Numbers: 18JC1413800, 20430713600, 18ZR1403900; National Natural Science Foundation of China, Grant/Award Numbers: 81872724, 81872895, 82073682

**Background and purpose:** PD-1/PD-L1 antibodies have achieved great success in clinical treatment. However, monoclonal antibody drugs also have challenges, such as high manufacturing costs, poor diffusion, low oral bioavailability and limited penetration into tumour tissue. The development of small-molecule inhibitors of PD-1/PD-L1 interaction represents a promising perspective to overcome the above challenges in cancer immunotherapy.

**Experimental approach:** We explored structural activity relationships and used biochemical assays to generate a lead compound (ZE132). CD8+ T-cells killing assay and *Irfng* expression assay were used to verify the *in vitro* cellular activity of ZE132. Off-target study was performed to verify the selectivity. Syngeneic mouse models were used to verify the *in vivo* activity of ZE132 in tumour immune microenvironment (TIME). We also performed pharmacokinetics profiling in mice and The Cancer Genome Atlas database analysis.

**Key results:** ZE132 can effectively inhibit the PD-1/PD-L1 interactions *in vitro*, and it has a potent affinity to PD-L1. ZE132 shows robust anti-tumour effects *in vivo*, better than anti-PD-1 antibody. In the analysis of TIME, we found that ZE132 treatment promotes cytotoxic T-cell tumour infiltration and induces IL-2 expression. In addition, ZE132 elicits strong inhibitory effects on the mRNA expression of TGF- $\beta$ , which may serve as a potential biomarker to predict responsiveness to PD-1/PD-L1 immunotherapies.

**Conclusion and implications:** We identified a new lead compound ZE132 targeting PD-1/PD-L1 interactions, not only showing favourable drug-like properties *in vitro* and *in vivo* but also showing the advantage of overcoming the barrier of TIME compared to anti-PD-1 antibody.

## KEYWORDS

immunotherapy, PD-1/PD-L1, TGF- $\beta$ , tumour immune microenvironment

**Abbreviations:** CTLA-4, cytotoxic T-lymphocyte-associated antigen-4; DCs, dendritic cells; IFN- $\gamma$ , interferon- $\gamma$ ; IL-10, interleukin 10; IL-2, interleukin 2; PD-1, programmed cell death-1; PD-L1, programmed cell death-ligand 1; PL-L2, programmed cell death-ligand 2; TGF- $\beta$ , transforming growth factor- $\beta$ ; TIME, tumour immune microenvironment.

Chenglong Liu and Feilong Zhou contributed equally.

## 1 | INTRODUCTION

Immune checkpoint molecules, such as **cytotoxic T-lymphocyte-associated antigen-4 (CTLA-4)**, **programmed cell death-1 (PD-1)** and **programmed cell death-ligand 1 (PD-L1)**, play key roles in inhibiting anti-cancer T-cell immunity in multiple cancers in humans (Zou et al., 2016). PD-1/PD-L1 blockade is a promising strategy in cancer therapy that has revolutionised the treatment of malignancies (Sun et al., 2020).

However, monoclonal antibody drugs also have caveats, such as immune-related adverse effects, high manufacturing costs, poor diffusion, low oral bioavailability and limited penetration into tumour tissue (Hwang et al., 2016; Naidoo et al., 2015). Current PD-1/PD-L1 humanised monoclonal antibodies were found to develop immunogenicity in humans (Hwang et al., 2016; Naidoo et al., 2015; Postow, 2015). Moreover, the large molecular weight of antibodies has disadvantages in membrane permeability, resulting in insufficient infiltration in solid tumours and comprising efficacy in clinical treatment (Perez et al., 2014). The development of small-molecule inhibitors of PD-1/PD-L1 interaction represents a promising perspective to overcome the above challenges in cancer immunotherapy.

Currently, several patent applications regarding small molecules targeting of PD-1/PD-L1 claim to be effective *in vivo* and *in vitro* (Miller et al., 2014; Sasikumar et al., 2012; Sharpe et al., 2011), however most of them are still in discovery and optimization stage. **AUNP12** was reported as the first peptide PD1/PDL1 inhibitor in 2014, with a structure similar to the PD-1 extracellular domain (Sasikumar et al., 2011). The shorter half-life of peptides reduces the occurrence of immune-related adverse reactions compared to antibodies. AUNP-12 contains 29 amino acids. Using HEK293 cells expressing hPD-L1 and hPD-1 for *in vitro* binding experiments, the EC<sub>50</sub> of AUNP-12 was 0.72 nmol·L<sup>-1</sup>, and in proliferation experiments, the EC<sub>50</sub> reached 0.41 nmol·L<sup>-1</sup> (Sasikumar et al., 2011; Sasikumar et al., 2019). In addition to AUNP12, **BMS-986189**, a macrocyclic peptide consisting of a 45-membered N-methylated backbone, entered the clinical phase in 2016 (Guzik et al., 2019).

In the field of small-molecule inhibitors of PD-1/PD-L1 interaction, **BMS-37** and **BMS-200** are early examples that inhibit this interaction *in vitro* (Guzik et al., 2017). One of the key structural features of BMS compounds is the biphenyl moiety, which is also observed in subsequently reported PD-1/PD-L1 inhibitors. For example, Gong et al. reported a biphenyl-containing compound **A22** inhibiting PD-1/PD-L1 interaction with an IC<sub>50</sub> value of 92.3 nmol·L<sup>-1</sup> *in vitro* (Qin et al., 2019). Furthermore, Basu et al. reported that the biphenyl-containing compound **2b** blocked PD1/PDL1 interaction with an IC<sub>50</sub> value of 3.0 nmol·L<sup>-1</sup> in a homogeneous time resolved fluorescence (HTRF) assay (Basu et al., 2019). Koneieczny et al. also reported a biphenyl-containing compound **2k** inhibited PD-1/PD-L1 interaction with an HTRF IC<sub>50</sub> value of 15.0 nmol·L<sup>-1</sup> and it induced PD-1 expression on CD4<sup>+</sup> and CD8<sup>+</sup> T-cells (Koneieczny et al., 2020). Despite the high *in vitro* potency observed for these biphenyl-containing compounds, their activities on T-cell immunity and *in vivo* anti-tumour activity remains understudied. Recently, **NP19**, a close analogue of BMS-37, has been investigated. It induced interferon- $\gamma$

### What is already known

- PD-1/PD-L1 antibodies have achieved great success in clinical treatment.
- Monoclonal antibody drugs have challenges in diffusion, oral bioavailability and penetration into tumour tissue.

### What this study adds

- A new lead compound-ZE132 was identified with robust anti-tumour effects, showing advantage over anti-PD-1.
- TGF- $\beta$  status links to potentially predicting responsiveness to PD-1/PD-L1 immunotherapies.

### Clinical significance

- ZE132 has the advantage of overcoming the barrier of tumour micromovement compared with antibody.
- ZE132 may be used to treat a wide range of cancers with anti-PD-1 resistance.

(IFN- $\gamma$ ) secretion from T-cells and inhibited tumour growth in the B16F10 melanoma mouse model (Cheng et al., 2020). Nevertheless, how small-molecule inhibitors of PD-1/PD-L1 interaction elicit their anti-tumour activity *in vivo* remains underexplored and warrants further studies.

Tumour cells can upregulate immune checkpoints to inhibit immune responses (Topalian et al., 2015). In the tumour immune microenvironment (TIME), PD-1/PD-L1 interaction can cause T-cell exhaustion and tumour cell immune escape (Hui et al., 2017; Patsoukis et al., 2012; Sharpe & Pauken, 2018). **Transforming growth factor- $\beta$  (TGF- $\beta$ )** in the tumour microenvironment drives immune evasion, which promotes T-cell exclusion (Tauriello et al., 2018). TGF- $\beta$  shapes the tumour microenvironment to restrain anti-tumour immunity by restricting T-cell infiltration. There is a significant correlation between the tumour mutational burden (TMB) and the objective response rate to PD-1 inhibition. Tumour mutational burden is one of the most widely used immunotherapy biomarkers to identify the patient response and predict therapeutic efficacy (Yarchoan et al., 2017). TGF- $\beta$  has been widely reported in immunosuppression in multiple cancers (Batlle & Massagué, 2019). In clinical trials, an anti-TGF- $\beta$  and anti-PD-L1 bispecific antibody shows encouraging anti-tumour efficacy (Bang et al., 2018).

In this study, we discovered a novel and potent small-molecule inhibitor of the PD-1/PD-L1 interaction, featuring a taurine and a biphenyl moiety. We systematically investigated the mechanism for this lead compound *in vivo* anti-tumour activity and its advantages over antibodies in modulating the TIME, as well as to better understand the biomarker related to treatment response.

## 2 | METHODS

### 2.1 | The AlphaLISA assay

The AlphaLISA assay was adopted with a commercial PD-1/PD-L1 Binding AlphaLISA Kit (PerkinElmer, #AL356C) following the manufacturer protocol. Briefly, a DMSO stock solution of the testing compound was serially diluted in EP tubes with 1× immunoassay buffer. These serially diluted working solutions were 4× concentration relative to the final testing solutions, and the volume added to each well is 10 µl. In addition, the His-tagged PD-L1 was diluted into a working protein solution to make it 4× concentration relative to the final testing solution. The same procedure was performed for the biotinylated tagged-PD-1. Subsequently, 10 µl of the working protein solution of the His-tagged PD-L1 and 10 µl of the working protein solution of the biotinylated tagged-PD-1 were added to each well accordingly. Finally, 10 µl of a freshly prepared mixture of 4× anti-His AlphaLISA acceptor beads and 4× Streptavidin donor beads was added, resulting in a final volume of 40 µl per well. The 384-well plate was incubated at room temperature in the dark for 90 min and the AlphaLISA signals were measured using an EnVision-Alpha Reader (PerkinElmer). The GraphPad Prism (RRID:SCR\_002798) was used to calculate the IC<sub>50</sub> values.

### 2.2 | Tumour cell lines

The cell lines EL4 (RRID:CVCL\_0255), 4T1 (RRID:CVCL\_0125), CT26 (RRID:CVCL\_7256), MC38 (RRID:CVCL\_B288) and B16F10 (RRID:CVCL\_0159) were purchased from the American Type Culture Collection (ATCC) and cultured according to the supplier's recommendations, supplemented with 10% foetal bovine serum (FBS) and penicillin-streptomycin solution at a concentration of 100 I.U.·ml<sup>-1</sup>.

### 2.3 | Animals

All animal care, ethical principles and experimental procedures conformed to the NIH Guide for the Care and Use of Laboratory Animals and were approved by the Department of laboratory animal science of Fudan University (Approval number: 2020-04-YL-ZD-02) (Shanghai, China). Animal studies are reported in compliance with the ARRIVE guidelines (Percie du Sert et al., 2020) and with the recommendations made by the British Journal of Pharmacology (Lilley et al., 2020). Ethical approval for experimentation that is recognised worldwide. The ethical review permissions were approved by the Institute for Research Ethics Committee in Fudan University and the studies were followed by institutional guidelines for the care and use of animals. Female C57BL/6, BALB/c and male Institute of Cancer Research (ICR) mice were purchased from Vital River Laboratories (Beijing, China). Male OT-I transgenic mice were purchased from Shanghai Model Organisms. The mice used in the experiments were 6–8 weeks old (18–20 g). Mice (2–3 mice per cage) were kept in

individually ventilated cages (transparent and with top filter-isolator) with standard bedding at a constant temperature of 23 ± 1°C and 40–60% humidity with 12 h light/darkness cycle in specific pathogen-free conditions with food and water at will. All the animal studies were designed to generate groups of equal size using randomisation and blinded analysis. The different group sizes are due to the purpose of multiple trials and unexpected individual losses during the process.

### 2.4 | Intradermal tumour establishment

C57BL/6 mice were inoculated subcutaneously (s.c.) with B16F10 (3 × 10<sup>5</sup>) or MC38 (1 × 10<sup>6</sup>) cells in the right flank on Day 0. BALB/c mice were inoculated s.c. with CT26 (3 × 10<sup>5</sup>) or 4T1 (3 × 10<sup>5</sup>) cells in the right flank on Day 0.

All cells were collected from the log phase of *in vitro* growth (~70% confluency). Any mouse without a developing tumour was excluded before grouping.

Three randomised cohorts (n = 5) with tumour size between 30 and 50 mm<sup>3</sup> were administered vehicle control (DMSO, i.p., QD) or anti-PD-1 (BioXcell, BE0146, Clone: RMP1-14, RRID:AB\_10949053) (10 mg·kg<sup>-1</sup>, i.p., BIW) or ZE132 (40 mg·kg<sup>-1</sup>, i.p., QD). The tumour growth and regression were determined using volume as the readout. The volumes (V) were calculated using the following formula:

$V = a * b * b/2$ , where a is the longest diameter and b is the shortest diameter.

Mice were killed (CO<sub>2</sub>, 5 min) either on at least Day 14 or when the tumour reached a maximum diameter of 15 mm. No surgical procedures and no anaesthesia were used for these studies. For each experimental procedure, prior to, during or after the experiments, animal welfare (e.g. humane end points) are included in the welfare-related assessments. The tumour samples were cut for flow cytometry, quantitative polymerase chain reaction (qPCR) and immunohistochemistry analysis. The serum was obtained for biochemical analysis. The plasma was collected for drug concentration analysis.

### 2.5 | Off-target study

#### 2.5.1 | The methods for testing compound inhibition activity against BCL-2/BIM, BCL-xL/BAK, MCL-1/BID and BFL-1/BID protein–protein interactions

The methods have been previously reported (Zhou et al., 2012). Briefly, the fluorescein tagged BIM (141-170), BAK (69-87) and BID (79-99) BH3 (Bcl-2 Homology 3) peptides, which were named FAM-BIM, FAM-BAK and FAM-BID, were synthesised from Synpeptide.com. Their K<sub>d</sub> values to BCL-2 (1-217), BCL-xL (1-209), MCL-1 (172-327) and BFL-1 (1-151) proteins were determined with a fixed concentration of FAM-BIM, FAM-BAK or FAM-BID, respectively, in saturation experiments. Based on our analysis of the dynamic ranges for the signals and their K<sub>d</sub> values, the proper pairs of the

fluorescein peptide (the tracer) and the protein were listed as follows: BCL2/FAM-BIM,  $K_d = 0.44 \text{ nmol}\cdot\text{L}^{-1}$ , BCL-xL/FAM-BAK,  $K_d = 12.55 \text{ nmol}\cdot\text{L}^{-1}$ ; MCL-1/FAM-BID,  $K_d = 10.4 \text{ nmol}\cdot\text{L}^{-1}$ ; BFL-1/FAM-BID,  $K_d = 0.81 \text{ nmol}\cdot\text{L}^{-1}$ .

In the competitive binding assay, the fluorescence polarisation values were measured using the Spark™ 10 M plate reader (Tecan U.S., Research Triangle Park, NC) in 96-well, black, round-bottom plates. To each single well, two components were added sequentially: (1) 4  $\mu\text{l}$  of the serial diluted testing compounds in DMSO; (2) To the assay buffer [100  $\text{mmol}\cdot\text{L}^{-1}$  potassium phosphate, pH 7.5, 100  $\mu\text{g}\cdot\text{ml}^{-1}$  bovine  $\gamma$ -globulin, 0.02% sodium azide and 0.01% Triton X-100; in case of MCL-1; Triton X-100 was replaced with PF68 (0.01%)], the tracer was added. Subsequently, the protein was also added to the assay buffer. Finally, 96  $\mu\text{l}$  of the assay buffer containing the tracer and the protein was added to each well. The final concentration of the tracer in each well is 5  $\text{nmol}\cdot\text{L}^{-1}$ . The final concentration of individual testing protein of interest is 20  $\text{nmol}\cdot\text{L}^{-1}$  for BCL-2, 50  $\text{nmol}\cdot\text{L}^{-1}$  for BCL-xL, 20  $\text{nmol}\cdot\text{L}^{-1}$  for MCL-1 or 20  $\text{nmol}\cdot\text{L}^{-1}$  for BFL-1. All the components were mixed in each well of the plates, which was incubated at room temperature for 1.5 h with gentle shaking. The polarisation values in millipolarisation units (mP) were measured at an excitation wavelength of 485 nm and an emission wavelength of 530 nm. The  $\text{IC}_{50}$  values were calculated with Graphpad.

### 2.5.2 | The methods for testing compound inhibition activity against MDM2/p53 and MDM2/p53 protein-protein interactions

MDMX (14-111, C17S) and MDMX (1-118) protein were expressed in *E. coli* and purified through nickel affinity chromatography and subsequently gel filtration chromatography. The FAM labelled PDI peptide (Hu et al., 2007) (FAM-PDI) was used as a tracer for both MDMX and MDM2 binding assay, and the  $K_d$  values tested for MDMX and MDM2 are 2.1 and 0.7  $\text{nmol}\cdot\text{L}^{-1}$ , respectively in the saturation experiments.

In the competitive binding assay, the fluorescence polarisation values were measured using the Spark™ 10 M plate reader in 96-well, black, round-bottom plates. To each single well, two components were added sequentially: (1) 4  $\mu\text{l}$  of the serial diluted testing compounds in DMSO; (2) To the assay buffer [10  $\text{mmol}\cdot\text{L}^{-1}$  Tris (pH 8.0) + 200  $\text{mmol}\cdot\text{L}^{-1}$  NaCl + 0.01% Tween20 + 0.01% TritonX-100 (MDMX); 100  $\text{mmol}\cdot\text{L}^{-1}$  potassium phosphate (pH 7.5) + 100  $\mu\text{g}\cdot\text{ml}^{-1}$  Bovine-r-globulin + 0.01% TritonX-100 (MDM2)], the tracer was added. Subsequently, the protein was also added to the assay buffer. Finally, 96  $\mu\text{l}$  of the assay buffer containing the tracer and the protein was added to each well. The final concentration of the tracer in each well is 5  $\text{nmol}\cdot\text{L}^{-1}$  in MDMX system and 2  $\text{nmol}\cdot\text{L}^{-1}$  in MDM2 system. The final concentration of individual testing protein of interest is 60  $\text{nmol}\cdot\text{L}^{-1}$  for MDMX or 20  $\text{nmol}\cdot\text{L}^{-1}$  for MDM2. All the components were mixed in each well of the plates, which was incubated at room temperature for 1.5 h with gentle shaking. The polarisation

values in millipolarisation units (mP) were measured at an excitation wavelength of 485 nm and an emission wavelength of 530 nm. The  $\text{IC}_{50}$  values were calculated with Graphpad.

### 2.5.3 | The methods for testing compound inhibition activity against TEAD2/YAP1 protein-protein interactions

TEAD2 (217-447) protein was expressed in *E. coli* and purified through nickel affinity chromatography and subsequently gel filtration chromatography. The FAM labelled YAP (60-99) mimetic (FAM-YAP) was used as a tracer, the peptide sequence of which is DSETDLEALFNAVMPNPKTANVPQTVPMLRKLPAFCKPP. The  $K_d$  values tested for TEAD2/FAM-YAP is 79.4  $\text{nmol}\cdot\text{L}^{-1}$  in the saturation experiments.

In the competitive binding assay, the fluorescence polarisation values were measured using the Spark™ 10 M plate reader in 96-well, black, round-bottom plates. To each single well, three components were added sequentially: (1) 5  $\mu\text{l}$  of the serial diluted testing compounds in the assay buffer (+20% DMSO); (2) 40  $\mu\text{l}$  of the assay buffer [1 $\times$  PBS pH 7.4 + 0.01% TritonX-100] containing TEAD2; (3) 40  $\mu\text{l}$  of the assay buffer containing the tracer. The final concentration of the tracer and TEAD2 in each well is 5 and 500  $\text{nmol}\cdot\text{L}^{-1}$ , respectively. All the components were mixed in each well of the plates, which was incubated at room temperature for 1.5 h with gentle shaking. The polarisation values in millipolarisation units (mP) were measured at an excitation wavelength of 485 nm and an emission wavelength of 530 nm. The  $\text{IC}_{50}$  values were calculated with Graphpad.

### 2.5.4 | The methods for testing compound inhibition activity against BRD2 BD1/BD2, BRD3 BD1/BD2 and BRD4 BD1/BD2

The methods have been previously reported, (Chen et al., 2019) which adopted herein without any changes.

### 2.5.5 | The methods for testing compound inhibition activity against BCL9/ $\beta$ -catenin

The method has been previously reported, (Kawamoto et al., 2009) which adopted herein without any changes.

## 2.6 | Immunohistochemistry

In immunohistochemistry analysis, CT26 tumour samples were used to analysis. Immunohistochemical procedures and analysis comply with the recommendations made by the *British Journal of Pharmacology* and adhere to the BJP checklist for and immunohistochemistry. Tumour samples were collected, fixed in 4% formalin for 24 h at 4°C, immersed

in 75% alcohol and embedded in paraffin. Anti-CD8 (ab209775; Abcam, RRID:AB\_2860566) was used for immunohistochemistry. Immunohistochemistry was performed using an Elivision Super HRP (Mouse/Rabbit), immunohistochemistry Kit (KIT-9922, Maixin Biotech) and a Catalyzed Signal Amplification System (K1500, Dako) according to the manufacturer's instructions. Each tissue section was analysed by using ImageJ software (ImageJ, RRID:SCR\_003070).

## 2.7 | H&E staining analysis

In *in vivo* toxicity experiment, C57BL/6 mice (6–8 weeks old) were randomly divided into three cohorts ( $n = 2$ ) and injected with vehicle control (DMSO, once a day/QD) or ZE132 (40 mg·kg<sup>-1</sup>, QD or 80 mg·kg<sup>-1</sup>, QD). At the end of 7 days of injection, mice were killed (CO<sub>2</sub>, 5 min). Various organs were collected and fixed with a 4% paraformaldehyde solution followed by embedding in paraffin and slicing into 5- $\mu$ m sections. The samples were stained with haematoxylin and eosin (H&E) and observed using Eclipse Ti microscope and NIS-Elements Color Cam Ver. 4.00 (Nikon, Japan).

## 2.8 | Pharmacokinetics profiling

Pharmacokinetics (PK) analysis of ZE132 was conducted in four male C57BL/6 SPF mice in accordance with the standard protocol (Viva Biotech) and ethical regulations (IACUC).

ZE132 (40 mg·kg<sup>-1</sup>) was administered through *i.p.* injection. Blood samples (300  $\mu$ l) were periodically collected at the retro-orbital vein at 0.083, 0.25, 0.5, 1, 2, 4, 8 and 24 h after dosing, followed by plasma separation for pending bioanalysis. Analytic concentrations were determined using LC-MS/MS (SCIEX Triple Quad™ 5500).

Concentrations of ZE132 were transformed to “power of 10” form for analysis.

## 2.9 | Flow cytometry analysis

At the end of the experiments, the termination of syngeneic murine models was performed, and tumours were cut and digested in a digestion cocktail (collagenase and deoxyribonuclease). Cells from the tumour were isolated and resuspended in PBS buffer.

For surface staining, antibodies targeting CD45(30-F11, RRID: AB\_1107002), CD8(53–6.7, RRID:AB\_1272185), PD-1(J43, RRID: AB\_465472), PD-L1(MIH5, RRID:AB\_466089), CD4(GK1.5,RRID: AB\_11157830), CD25(PC61.5, RRID:AB\_465607), CD11c(N418, RRID:AB\_1548654), CD11b(M1/70, RRID:AB\_469588), CD103(2E7, RRID:AB\_465799), and MHC II(M5/114.15.2,RRID:AB\_469455) were purchased from eBioscience.

After surface staining, cells were fixed and permeabilized using the FoxP3/Transcription Factor Staining kit (5523-00, eBioscience). Antibodies targeting IFN- $\gamma$  (XMG1.2,RRID:AB\_466193), Granzyme B (NGZB,RRID:AB\_11149362), IL-2 (JES6-5H4,RRID:AB\_469490),

Foxp3 (FJK-16S,RRID:AB\_469457) and CXCL9 (MIG-2F5.5,RRID: AB\_11218694) were purchased from eBioscience. Flow cytometry data were acquired on FACS Aria II (BD) and analysed using FlowJo software (RRID:SCR\_008520). Data from different batches were normalised within FlowJo CytoNorm.

## 2.10 | HTRF assay

PD-1/PD-L1 Binding Assay Kit (Cisbio, #641CP01PEG) was used in HTRF assays. Dilution buffer was used to dilute the compound dissolved in DMSO into a working sample solution, and 12 gradients were set. The working sample solution was 10 $\times$  concentrated relative to the testing sample solution.

Tag1-PDL1 and Tag2-PD1 were diluted into a working protein solution. The working protein solution was 5 $\times$  concentrated relative to the testing protein solution.

Anti-Tag1-Eu3 and Anti-Tag2-XL665 were mixed in a ratio of 1:1.

First, 2  $\mu$ l of the compound solution was added to a 96-well plate. Then, 4  $\mu$ l of a Tag1-PDL1 and Tag2-PD1 mix was added. After an incubation step of 15 min, 10  $\mu$ l per well of the Anti-Tag1-Eu3 and Anti-Tag2-XL665 mixture was added, resulting in a final volume of 20  $\mu$ l per well.

After another 30 min incubation at room temperature, the samples were measured using a Microplate Reader (SPARK 10 M, TECAN; excitation, 320 nm; emission, 650 and 612 nm). The final HTRF ratio was calculated as: ratio = (signal 650 nm/signal 612 nm)  $\times$  10,000. GraphPad was used to calculate the IC<sub>50</sub> of the compounds.

## 2.11 | Biacore assay

hPD-L1(Genscript, Z03371), hPD-L2(Genscript, Z03417) or hPD-1 (Genscript, Z03370) were immobilised on a CM5 chip (GE Health) by using Biaore T200.

Sensogram was obtained by using a series of different concentrations of ZE132 (40,000, 20,000, 10,000, 5000, 2500, 1250, 625, 312.5, 156.25, 78.125, 39.0625, 19.53 and 9.76 nmol·L<sup>-1</sup>). SPR sensorgrams have association time intervals of 45 s and dissociation time intervals of 60 s. Data were analysed by using Biacore Evaluation Software.

## 2.12 | Cell Counting Kit-8 and lactate dehydrogenase assays

Cell proliferation was estimated using the Cell Counting Kit-8 and lactate dehydrogenase assay. EL4 cells were used for the logarithmic growth phase. Cell suspensions ( $2 \times 10^4$  cells per well) were added to 96-well plates in a volume of 100  $\mu$ l per well. The treatment, solvent control and control groups were treated with different concentrations of ZE132 using the corresponding solvent (DMSO) or culture media. The final concentrations of ZE132 were 10 and 1  $\mu$ mol·L<sup>-1</sup>.

Each group was prepared with three parallel wells and incubated at 37°C and 5% CO<sub>2</sub> for 48 h.

In the Cell Counting Kit-8 assay, 10 µl Cell Counting Kit-8 (MA0218, Meilunbio) was added to each well at the end of the culture period. After a 2 h incubation step, the absorbance was measured with Synergy H1 (BioTek).

The lactate dehydrogenase assay was performed using a lactate dehydrogenase cytotoxicity detection kit (C0016, Beyotime), and all procedures were performed according to the supplier's recommendations. The absorbance was measured using Synergy H1 (BioTek).

## 2.13 | T-cell cultures

OVA-specific CD8<sup>+</sup> cytolytic T-cells were generated by incubating OT-I mice splenocytes with 10 µg·ml<sup>-1</sup> SIINFEKL peptide (Sangon Biotech, T510212) and 20 ng·ml<sup>-1</sup> mL-2(R&D systems, 402-ML) for 5–7 days. At the end of culture, the culture contained >95% cytotoxic T-cells (Gropper et al., 2017; Taylor et al., 2016).

## 2.14 | OT-I T-cell cytotoxicity assay

EL4 cells were treated with compounds at different concentrations for 24 h. DMSO and anti-PD-L1 (BioXcell, BE0101, Clone:10F.9G2, RRID:AB\_10949073) were used as the vehicle and positive control, respectively. Then, EL4 cells were harvested and resuspended in RPMI-1640 medium at 1 × 10<sup>6</sup> cells·ml<sup>-1</sup>.

EL4 cells were pulsed with medium vehicle control or 10 mg·ml<sup>-1</sup> SIINFEKL peptide for 2 h at 37°C and then labelled with 0.25 or 5 mmol·L<sup>-1</sup> CFSE (Thermo Fisher Scientific, #C34554) for 10 min at 37°C, respectively. The EL4 cells were co-cultured with CD8<sup>+</sup> T-cells isolated from splenocytes of C57BL/6 mice at different E:T ratios for 12 h. Compounds in different concentrations were added to the culture medium. After incubation, the percentage of specific killing was determined by flow cytometric analysis (Beckman CytoFlex S).

Specific killing (%) = [1-Sample ratio/Negative control ratio] \* 100;

Sample ratio = [CFSE high (EL4 pulsed with OVA)/CFSE low (vehicle control)] value of each sample co-cultured with CD8<sup>+</sup> T-cells;

Negative control ratio = [CFSE high (EL4 pulsed with OVA)/CFSE low (vehicle control)] value of EL4 cells not co-cultured with CD8<sup>+</sup> T-cells.

The killing efficiency of vehicle group was used as the baseline.

## 2.15 | Small interfering RNA transfection

For small interfering RNA (siRNA) knockdown, 4 × 10<sup>4</sup> cells·ml<sup>-1</sup> EL4 cells were cultured in 24-well plate for 12 h before transfection. Diluting 2 µl of Lipofectamine 2000 (Thermo, 11,668,019) with 25 µl of Opti-MEM and diluting 500 ng of siRNA with 25 µl of Opti-MEM. Next, the diluted Lipofectamine 2000 and diluted siRNA were mixed

and incubated for 20 min. Non-targeting siRNA was used as negative control. The mRNA expression level of *Cd274* was measured by qPCR after 48 h.

siRNA Sequence:

*Cd274*-siRNA1:

sense:5' GGCGUUUACUGCUGCAUAATT 3';

anti-sense:5' UUAUGCAGCAGUAAACGCCTT 3'.

*Cd274*-siRNA2:

sense:5' GAGGUAUCUGGACAAACATT 3';

anti-sense:5' UGUUUGUCCAGAUUACCUCTT 3'.

*Cd274*-siRNA3:

sense:5' GGAGAAAUGUGGCGUUGAATT 3';

anti-sense:5' UUCAACGCCACAUUUCUCCTT 3'.

## 2.16 | Effects of ZE132 on *Ifng* expression in OT-I CD8<sup>+</sup> T-cells in vitro

After 3 days of culture with SIINFEKL peptide and IL-2 (as mentioned earlier), OT-I CD8<sup>+</sup> T-cells were plated in the 24-well plate with a density of 2 × 10<sup>6</sup> cells per well in 500 µl 1640-RPMI containing 10% FBS with or without mPD-L1(Abcam, ab130039) protein (25 and 50 nmol·L<sup>-1</sup>). Then 1 and 10 µmol·L<sup>-1</sup> ZE132 were added to the wells, respectively, and cultured at 37°C for 24 h. Then the CD8<sup>+</sup> T-cells were collected for detecting of *Ifng* expression by using qPCR.

## 2.17 | Reverse transcription and quantitative real-time PCR

Total RNA (500 ng) was isolated from cells using Trizol (Thermo, #11596026) and reverse-transcribed to complementary DNA using Evo M-MLV reverse transcription (RT) Premix (AG11706, Accurate Biology). Complementary DNA was then diluted and used for quantification by quantitative PCR, which was performed using SYBR® Green Premix Pro Taq (AG11701, Accurate Biology) and the StepOne-Plus real-time PCR system (Applied Biosystems).

Primer Sequence:

*Gapdh*:

F 5' AGGTCGGTGTGAACGGATTG 3';

R 5' TGTAGACCATGTAGTTGAGGTC 3'.

*Cxcl9*:

F 5' GGAGTTCGAGGAACCCTAGTG 3';

R 5' GGGATTTGTAGTGGATCGTGC 3'.

**Cd8:**

F 5' CCGTTGACCCGCTTTCTGT 3';  
R 5' CGGCGTCCATTTTCTTTGGAA 3'.

**Havcr2:**

F 5' TCAGGTCTTACCCTCAACTGTG 3';  
R 5' GGGCAGATAGGCATTTTTACCA 3'.

**Ifng:**

F 5' ATGAACGCTACACACTGCATC 3';  
R 5' CCATCCTTTTGGCAGTTCCTC 3'.

**Il2:**

F 5' TGAGCAGGATGGAGAATTACAGG 3';  
R 5' GTCCAAGTTCATCTTCTAGGCAC 3'.

**Tgfb1:**

F 5' CTCCCGTGGCTTCTAGTGC 3';  
R 5' GCCTTAGTTTGGACAGGATCTG 3'.

The results of RT-PCR were transformed to the form of “fold change” to show the different mRNA expression level between treatment group and control group.

## 2.18 | Serum biochemical analysis

BALB/c mice inoculated subcutaneously (s.c.) with CT26 were used here. After treatment, BALB/c mice were killed by CO<sub>2</sub> inhalation and blood was immediately collected in a sodium citrate tube and centrifuged at 5000 xg for 10 min. Serum was stored at -80°C for subsequent alanine aminotransferase (ALT), aspartate aminotransferase (AST), total and direct bilirubin, albumin (ALB) and alkaline phosphatase (ALP) measurements.

## 2.19 | Bioinformatics analysis

RSEM-normalised gene expression and clinical data from breast invasive carcinoma, colon adenocarcinoma and skin cutaneous melanoma patients were downloaded from The Cancer Genome Atlas Program (RRID:RRID:SCR\_003193) data portal. The Cancer Genome Atlas datasets, including colon adenocarcinoma and READ, were downloaded from cBioPortal (<http://www.cbioportal.org/>, RRID:SCR\_014555). The expression data from these patients were uploaded to Cibersort web server as mixed files. Default parameters were applied.

The samples were divided into high and low expression groups based on gene median expression levels. The datasets were analysed

in KM-plot (<http://kmplot.com>) and were divided into high and low expression groups based on gene median expression levels. A Kaplan-Meier curve was constructed to compare the overall and disease-free survival rates in the two groups. LogRank *p* value and HR were calculated with SPSS v 16.0. Kaplan-Meier overall survival curves of breast invasive carcinoma (Figure S7a) and skin cutaneous melanoma (Figure S7b) patients in different subgroups based on **transforming growth factor beta-1 (TGFB1)** gene expression levels. LogRank *p* value and HR were calculated with SPSS v 16.0 (RRID:SCR\_019096).

GSE141119 data set was used. These data include melanoma patients with anti-PD-1 treatment and the patient's tumour RNA-Seq dataset. We selected the PD-1 expression cell group for analysis, to investigate the treatment the relationship between the expression of *PDCD1* (PD-1 gene) and *TGFB1* before treatment (T0) and after treatment (M1, M2).

## 2.20 | Statistical analysis

The data and statistical analysis comply with the recommendations of the British Journal of Pharmacology on experimental design and analysis in pharmacology (Curtis et al., 2018). Additional data from different models were provided to validate the results. In our analysis, the size of independent groups was at least 5 (exact numbers are provided in the figure legends). We did not perform statistical analysis for small groups, and their results are only exploratory and preliminary. Results are expressed as mean ± SEM. Data were analysed by Student's *t*-test when comparing two groups. Among multiple groups, one-way ANOVA with Tukey's test was conducted for comparisons. Post hoc tests were run only if *F* achieved *p* < .05, and there was no significant variance inhomogeneity. *P* values < .05 were considered statistically significant, and all tests were two-tailed. When outliers were included or excluded in analysis, this is stated within the figure legend. Log-transformation and data normalisation methods were used to analysis.

All statistical analyses were performed using GraphPad Prism 8 (GraphPad Software, La Jolla, CA, USA, RRID:SCR\_002798).

All studies followed the editorial on experimental design and analysis in pharmacology (Curtis et al., 2018) and followed the BJP checklist for Design and Analysis.

## 3 | MATERIALS

AlphaLISA Kit(#AL356C) was from PerkinElmer. PD-1/PD-L1 Binding Assay Kit (HTRF)(#64ICP01PEG) was from Cisbio. Immunohistochemistry kit(#KIT-9922) was from Maixin Biotech. CM5 chip(#29149603) was from GE Health. Evo M-MLV RT Premix(#AG11706) and SYBR® Green Premix Pro Taq(#AG11701) were from Accurate Biology (Changsha, China). Trizol(#11596026), Lipofectamine 2000 (#11668019) and CFSE(#C34554) were from Thermo. SIINFEKL peptide(T510212) was from Sangon Biotech (Shanghai, China). mL-2

(#402-ML) was from R&D Systems (Minneapolis, MN, USA). hPD-1 (#Z03370), hPD-L1(#Z03371) and hPD-L2(#Z03417) were from Genscript (Nanjing, China). Cell Counting Kit-8 assay kit(#MA0218) was from Meilunbio (Dalian, China) and lactate dehydrogenase assay kit(#C0016) was from Beyotime (Shanghai, China).

Antibodies targeting CD45(30-F11, RRID:AB\_1107002), CD8 (53-6.7, RRID:AB\_1272185), PD-1(J43, RRID:AB\_465472), PD-L1 (MIH5, RRID:AB\_466089), CD4(GK1.5, RRID:AB\_11157830), CD25 (PC61.5, RRID:AB\_465607), CD11c(N418, RRID:AB\_1548654), CD11b(M1/70, RRID:AB\_469588), CD103(2E7, RRID:AB\_465799), MHC II(M5/114.15.2, RRID:AB\_469455), IFN- $\gamma$  (XMG1.2, RRID:AB\_466193), Granzyme B (NGZB, RRID:AB\_11149362), IL-2 (JES6-5H4, RRID:AB\_469490), Foxp3 (FJK-16S, RRID:AB\_469457) and CXCL9 (MIG-2F5.5, RRID:AB\_11218694) were purchased from eBioscience. ZE138 (2-((5-Chloro-2-((5-cyanopyridin-3-yl)methoxy)-4-((3-(2,3-dihydrobenzo[b][1,4]dioxin-6-yl)-2-methylbenzyl)oxy)benzyl)(3-(dimethylamino)propyl)amino)ethane-1-sulfonic acid) and analogues synthesis and nuclear magnetic resonance (NMR) spectra are shown in supporting Data S.

### 3.1 | Nomenclature of targets and ligands

Key protein targets and ligands in this article are hyperlinked to corresponding entries in the IUPHAR/BPS Guide to PHARMACOLOGY <http://www.guidetopharmacology.org>, and are permanently archived in the Concise Guide to PHARMACOLOGY 2019/20 (Alexander et al., 2019).

## 4 | RESULTS

### 4.1 | ZE132 can effectively improve the *in vitro* cytotoxic killing of T-cells

In order to evaluate small molecules that competitively inhibit PD-1/PD-L1 interaction *in vitro*, we used AlphaLISA test. Structures of series compounds are shown in Figure 1a. Synthesis methods and nuclear magnetic resonance spectra are shown in supporting information related to Figure 1. We incorporated a taurine moiety into the modified biphenyl core structure of BMS200 and synthesised **1** (ZD45), which has a PD-1/PD-L1 inhibitory IC<sub>50</sub> value of 6.06 nmol·L<sup>-1</sup> (Figure 1b). Its close analogue **2** (ZD39), comprising of a homotaurine moiety, inhibited PD-1/PD-L1 interaction with an IC<sub>50</sub> value of 1.86 nmol·L<sup>-1</sup>. However, both **1** and **2** have very poor solubility in DMSO and aqueous solution, and are not suitable for further biological evaluations. In order to improve their aqueous solubility, side chains were incorporated and **3** (ZE132) and **4** (ZE131) were synthesised, which also inhibited PD-1/PD-L1 interaction with IC<sub>50</sub> values of 23.49 and 35.03 nmol·L<sup>-1</sup>, respectively. **5**(BMS-1266), a compound reported in a patent, was included as a positive control, which inhibited PD-1/PD-L1 interaction with an IC<sub>50</sub> value of 32.23 nmol·L<sup>-1</sup>. In addition, we also used Cisbio's HTRF binding-

affinity test (Figure S1a). These data suggested that the taurine moiety is beneficial for optimal *in vitro* potency.

To further investigate the role of ZE132 in blocking the PD-1/PD-L1 pathway, we used Biacore assay to explore the possible mechanism. Data showed that ZE132 has a strong affinity with PD-L1 and the KD value is 19.36 nmol·L<sup>-1</sup> (Figure 1c), which is consistent with the results from AlphaLISA and HTRF assays. ZE132 has weaker affinity with PD-L2 and has no affinity with PD-1(Figure S1b,c).

In order to examine whether ZE132 also blocks other protein-protein interactions, we tested it in 13 protein-protein interaction assays, including BRDs/Histone, MDM2/p53, MDMX/p53, TEAD2/YAP1, BCL2/BIM, MCL1/BID, BCL2/BAK and BFL1/BID, using the corresponding effective inhibitors as positive controls. The results showed that ZE132 did not elicit off-target effects, indicating it has good selectivity (Figure S2a-m).

Subsequent *in vitro* cytotoxic killing experiments were performed to verify the compounds activities at the cellular level. In many studies, CFSE killing assay has been widely used to detect the *in vitro* killing activity of cytotoxic T-cells (Gropper et al., 2017; Taylor et al., 2016), so the OT-I CFSE cytotoxic cell assay was adopted where the PD-L1 antibody was used as a positive control. Briefly, OT-I genetically modified mouse splenocytes and EL4 mouse lymphoma cells were harvested for the experiments. To test whether EL4 cells are suitable for verifying cell killing after blocking PD-1/PD-L1 signaling, we used antibodies to block PD-L1 on the surface of EL4 cells. Using flow cytometry analysis, we found EL4 cell surface expression of PD-L1, suitable for compound-killing detection (Figure 1d). As shown in Figure S3d, **4** (ZE131) were inactive, indicating the necessity of the taurine moiety and the basic side chain for optimal cellular activity. **In addition, 3 (ZE132) killed EL4 cells in a dose-dependent manner and showed a higher tumour cell killing potency at 10  $\mu\text{mol}\cdot\text{L}^{-1}$  with a 2:1 E:T ratio compared to that of PD-L1 antibodies (Figure 1e).** killing assay data of other compounds were shown in Figure S3a-e. These data suggested that the taurine moiety is beneficial for optimal cellular potency. Therefore, ZE132 was chosen as the lead compound for further characterisation.

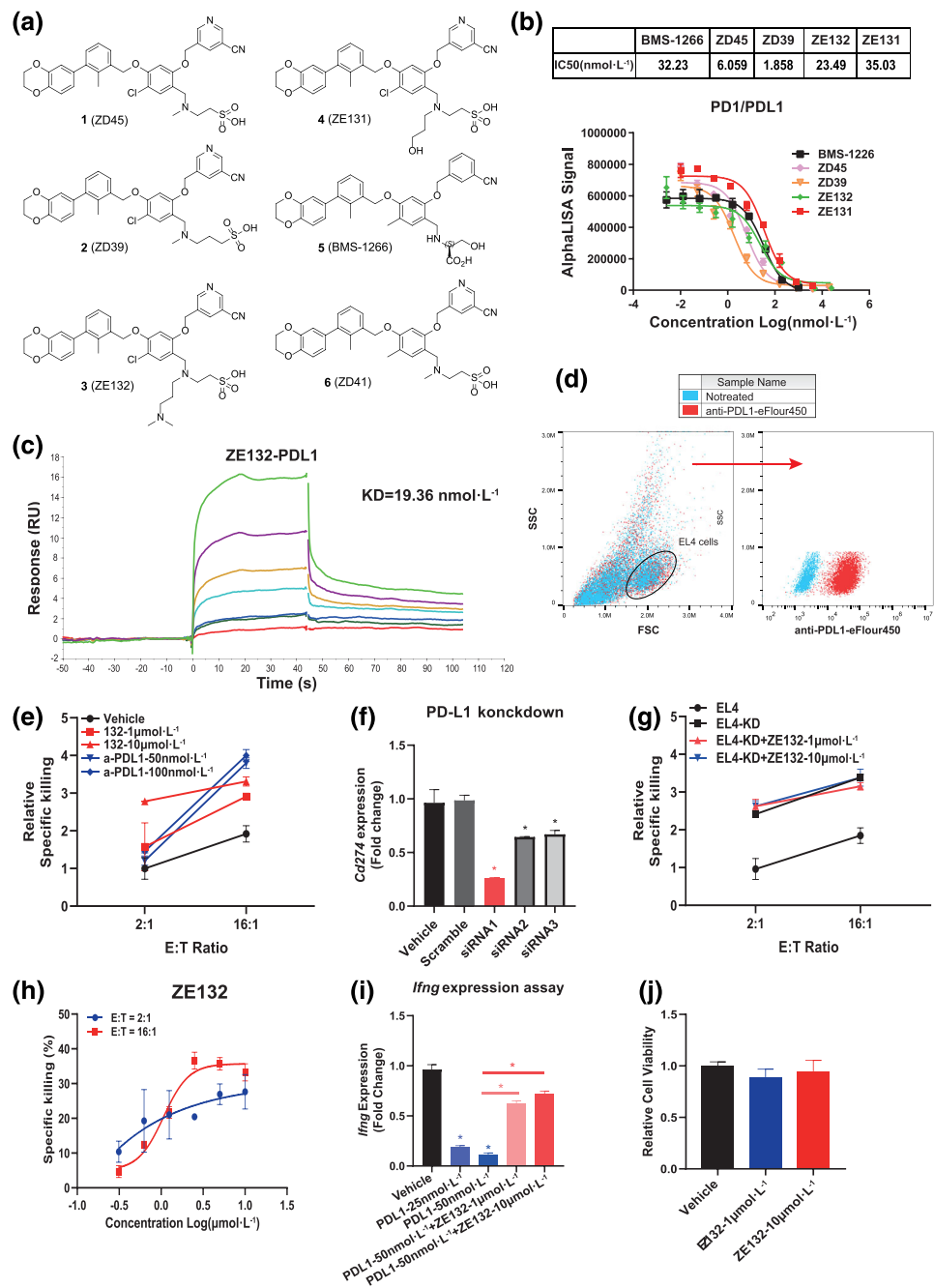
When using siRNA to knock down the Cd274 mRNA expression level of EL4 cells, the effect of ZE132 on improving the killing effect of OT-I CD8+ T-cells disappeared (Figure 1f-g). Subsequently, we used more concentration gradients to make the curve of killing assay, and vehicle cohort was used as baseline (Figure 1h).

In the experiment, it was found that PD-L1 protein could activate the PD-1/PD-L1 pathway in CD8+ T-cells and inhibit the mRNA expression of *Irfng* in T-cells. Under treatment of ZE132, the mRNA expression level of *Irfng* in T-cells was significantly increased, and there was a concentration dependent effect. It was proved that ZE132 could effectively block the PD-1/PD-L1 interaction (Figure 1i).

To detect the specificity of the compound and whether the proliferation inhibition of EL4 is due to non-immune-induced cytotoxicity to cells, we used Cell Counting Kit-8 assay and lactate dehydrogenase experiments to detect the effect of the compound on cytotoxicity. The results showed that ZE132 had no significantly toxic effect to tumour cells alone at concentrations of 1 and 10  $\mu\text{mol}\cdot\text{L}^{-1}$  (Figures 1j

### FIGURE 1 Structure/activity relationship and lead optimization.

(a) The structure of a series of compounds targeting PD-1/PD-L1 interaction. BMS-1266 is from a publicly available patent of Bristol Myers Squibb. (b) AlphaLISA assay results in vitro. Customised AlphaLISA assay detecting inhibition between biotinylated tagged-PD-1 and His-tagged PD-L1. ZE132 is screened as an active compound ( $IC_{50} = 23.49 \text{ nmol}\cdot\text{L}^{-1}$ ). (c) Sensorgram and saturation curve of the titration of ZE132 on hPD-L1 immobilised on a CM5 chip. The binding curve was fit to get a  $KD$  value of  $19.36 \text{ nmol}\cdot\text{L}^{-1}$  (concentration gradients: 1250, 500, 250, 125, 31.25, 15.625, and  $7.8125 \text{ nmol}\cdot\text{L}^{-1}$ ). Data were calculated by using Biacore T200 software. (d) Flow cytometry measurement of surface PD-L1 expression in EL4 cells. Cells treated or untreated anti-PD-L1 were measured respectively, and the images were finally compared by overlapping. (e) OT-I mice cytotoxic T-cells were used to detect the activity of compounds in vitro. Different ZE132 concentrations and E:T ratios were used to prove the activity of ZE132, and anti-PD-L1 was used as a positive control. The killing efficiency of vehicle group (E:T = 2:1) was used as the baseline. (f) qPCR analysis of *Cd274* mRNA expression in EL4 cells after silenced by siRNA (\* $p < .05$ ). (g) The killing effect of OT-I CD8+ T-cells on EL4-Cd274KD cells under ZE132 treatment. (h) Dose-response curves of killing efficiency of ZE132 in vitro killing assay (the killing efficiency at concentration of 0 was used as the baseline). (i) OT-I CD8+ T-cells were plated in a 24-well plate with or without mPD-L1. Then, ZE132 with different concentrations was added to the wells and cultured for 24 h. Cells were collected for detection of *Ifng* mRNA expression by using qPCR. (j) Cytotoxicity of ZE132 treatment in EL4 cells, measured by Cell Counting Kit-8 assay. EL4 cells were treated with 1 or  $10 \mu\text{mol}\cdot\text{L}^{-1}$  ZE132 over 24 h. Statistical significance of differences between groups was determined by unpaired Student's t-test. All data are presented as mean  $\pm$  SD of five independent experiments with triplicate



and S3f). The toxicity data of other compounds were shown in Figure S3g,h. These data show that cell growth inhibition during *in vitro* OT-I cytotoxic experiments was caused by T-cell killing rather than compounds directly killing tumour cells.

Taken together, aforementioned results indicated that the compound ZE132 can effectively block PD-1/PD-L1 interaction, effectively alleviate the resulting T-cell depletion and improve T-cell killing efficiency.

#### 4.2 | *In vivo* efficacy of ZE132 in mouse models

To test the *in vivo* efficacy of ZE132, we used four syngeneic mouse models (B16F10, CT26, MC38 and 4T1). Following s.c. inoculation of tumour cells, mice were treated with ZE132 to validate anti-tumour effects *in vivo*.

BMS-1266 and ZD41, which are derivatives of ZE132, showed significant anti-tumour effects in the B16F10 model (Figure S4a). Next, we optimised ZD41 into ZE132 for *in vivo* experiments.

ZE132 was first tested in the B16F10 model (Figure 2a). The picture of B16F10 tumour volume was shown in Figure S4b. Mice were grouped according to the administration regimen as follows: the vehicle control group, PD-1 antibody group (i.p. 10 mg·kg<sup>-1</sup> BIW), PD-L1 antibody group (i.p. mg·kg<sup>-1</sup>BIW) and ZE132 group (i.p. 20 mg·kg<sup>-1</sup> or 40 mg·kg<sup>-1</sup>QD). The compound ZE132 showed a dose-dependent effect and the tumour growth inhibition rate was equal to or higher than that of the antibody group.

ZE132 was also assessed in the CT26 mouse colorectal cancer model established in immunocompetent mice (regular BALB/c). The mice were grouped according to the administration regimen as follows: blank control, PD-1 antibody group (i.p. 10 mg·kg<sup>-1</sup>BIW) and ZE132 group (i.p. 40 mg·kg<sup>-1</sup>QD). ZE132 showed anti-tumour effects, with a tumour growth inhibition of 64%, which is better than PD-1 antibody in the same model (tumour growth inhibition of 38%) (Figure 2b). The picture of CT26 tumour volume is shown in Figure S4c. The MC38 and 4T1 models were also used to detect the anti-tumour effects of ZE132. In the MC38 model, ZE132 showed a similar anti-tumour effect to the previous two models (Figure 2c). In contrast, tumour growth inhibition in the 4T1 immune-competent model was low (Figure 2d). The pictures of tumour volume 4T1 models were shown in Figure S4d.

In summary, ZE132 and its derivatives exhibited robust anti-tumour effects *in vivo* by targeting PD-1/PD-L1 signalling, and these effects were more pronounced in CT26 and B16F10 models.

#### 4.3 | ZE132 lead compound demonstrates favourable PK profiles

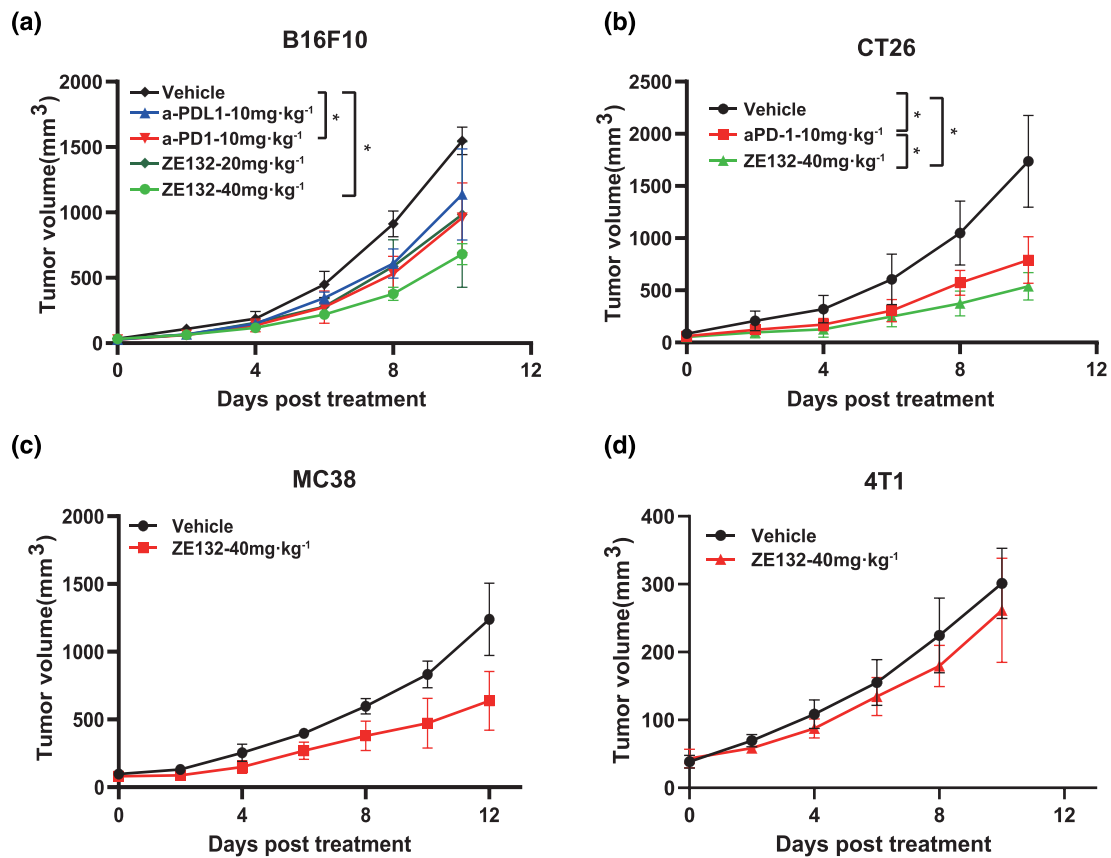
In addition to *in vitro* and *in vivo* efficacy, substantial improvement of pharmacological features was a major goal of our lead optimization. Pharmacokinetic experiments were conducted in C57BL/6 mice (Figure 2e). After i.p. injection of ZE132 at 40 mg·kg<sup>-1</sup>, sampling at

different time points showed a half-life of 1.6 ± 0.4 h and a clearance rate of 7679 ± 1840 ml·h<sup>-1</sup>·kg<sup>-1</sup>, indicating favourable metabolic conditions. In addition, ZE132 demonstrated favourable bioavailability and half-life properties, indicating the feasibility of daily dosing. ZE132 administered at 40 mg·kg<sup>-1</sup> via i.p. injection yielded a C<sub>max</sub> in plasma ranging from 1829 ± 893 ng·ml<sup>-1</sup>, much greater than the compound's *in vitro* IC<sub>50</sub> in cellular assays. Furthermore, ZE132 resulted in AUC values in plasma spanning of 5204 ± 1350 h·nmol·ml<sup>-1</sup> (Figure 2e). ZE132 had a low rate of clearance, ranging from 7.68 ± 1.84 L·h<sup>-1</sup>·kg<sup>-1</sup>, and an apparent volume of distribution (V<sub>d</sub>), ranging from 18.1 ± 9.12 L·kg<sup>-1</sup>. Both the low clearance and extended half-life of ZE132 in mice suggest that effective exposure levels are achievable at therapeutic doses in humans. The pharmacokinetic data of ZE132 i.v. 20 mg·kg<sup>-1</sup> in ICR mice were shown in Figure S4e. In summary, ZE132 showed good pharmacokinetic characteristics *in vivo*.

#### 4.4 | ZE132 enhances the tumour growth inhibition of cytotoxic lymphocytes by blocking PD-1/PD-L1 interaction

Previous studies reported that PD-1/PD-L1 blocking promotes cytotoxic lymphocyte activity by increasing the secretion of cytokines such as interferon-γ (IFN-γ) and interleukin 2 (IL-2) (Butte et al., 2007). To analyse the mechanism of tumour growth inhibition of ZE132 *in vivo*, we performed an analysis of key tumour-infiltrating immune cells and cytokine expression levels. Flow cytometry analysis of tumours was performed on tumour tissue after treatment to analyse immune cell changes in the TIME and related gating strategy are shown in Figure 3a. After tumour dissection, tumour tissue samples were processed into a single-cell suspension, followed by antibody staining. In B16F10 and CT26 models, IFN-γ<sup>+</sup>, IL-2<sup>+</sup> and granzyme B + CD8<sup>+</sup> cytotoxic T-cell tumour infiltration was significantly increased compared with the PD-1 antibody group and vehicle group after ZE132 treatment, indicating that the function of cytotoxic T lymphocytes in TIME was restored, increasing the cytotoxic effect of T-cells to tumour cells (Figures 3b–d and S4f–h). We also took advantage of quantitative PCR (qPCR) to examine the cytokine expression levels in tumours. qPCR results showed a significant increase in expression of the *Ifng* and *Il2* mRNA expression upon ZE132 treatment in B16F10 model (Figure 3e,f). A similar increase in expression of the *Ifng* and *Il2* mRNA expression can also be observed in the CT26 model treated with ZE132 compared with vehicle (Figure S4i,j).

Additionally, upon PD-1 antibody or ZE132 treatment, regulatory T-cells, which promote tumour growth by inhibiting the function of cytotoxic CD8<sup>+</sup> T-cells and play an inhibitory role in TIME, shows decreased tumour infiltration in B16F10 model and these results indicate TIME changes favouring immune reactions (Figure 3g,h). A similar decrease of regulatory T-cells tumour infiltration can also be observed in the CT26 tumour treated with ZE132 compared to that of vehicle (Figure S4k).



(e)

	$t_{1/2}$ (h)	$T_{max}$ (h)	$C_{max}$ (ng·mL <sup>-1</sup> )	$AUC_{(0-t)}$ (h·ng·mL <sup>-1</sup> )	$AUC_{(0-\infty)}$ (h·ng·mL <sup>-1</sup> )	$MRT_{(0-t)}$ (h)	$MRT_{(0-\infty)}$ (h)	Vd (mL·kg <sup>-1</sup> )	CL (mL·h <sup>-1</sup> ·kg <sup>-1</sup> )
i.v.	0.7±0.1	0.1±0	114934.2±39810.5	19614.5±4759.8	19626.3±4757.5	0.4±0.1	0.5±0.1	2152.9±626.5	2129.8±505.8
i.p.	1.6±0.4	1.5±0.6	1829.3±893.6	5204.1±1349.7	5437.3±1287.8	2.8±0.5	2.9±0.5	18095.8±9115.3	7679.0±1840.3

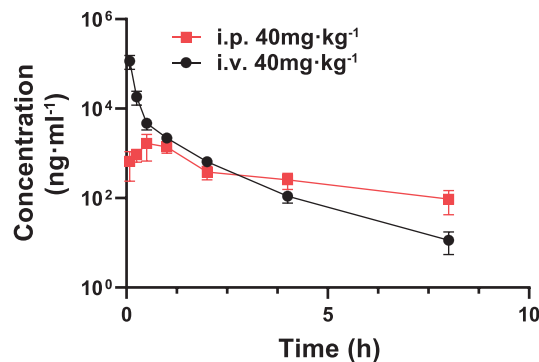


**FIGURE 2** *In vivo* efficacy of ZE132 in mice. (a) C57BL/6 mice were inoculated B16F10 cells via single flank implantation and treated with vehicle control, ZE132 (20 or 40 mg·kg<sup>-1</sup>, i.p., QD), anti-PD-1 (10 mg·kg<sup>-1</sup>, i.p., BIW) and anti-PD-L1 (10 mg·kg<sup>-1</sup>, i.p., BIW) via i.p. injection after tumour volume reached 30 mm<sup>3</sup> (n = 5 per cohort) (\**p* < .05). (b) BALB/c mice were inoculated CT26 cells via single flank implantation and treated with a vehicle control, ZE132 (40 mg·kg<sup>-1</sup>, i.p., QD) and anti-PD-1 (10 mg·kg<sup>-1</sup>, i.p., BIW) via i.p. injection after tumour volume reached 30 mm<sup>3</sup> (n = 5 per cohort) (\**p* < .05). (c) MC38 cells were inoculated into C57BL/6 mice before treatment with a vehicle control, ZE132 (40 mg·kg<sup>-1</sup>, QD), and anti-PD-1 (10 mg·kg<sup>-1</sup>, BIW) via i.p. injection. After treatment, tumour samples were cut and displayed to show the volume difference (n = 4 per cohort). (d) BALB/c mice were inoculated 4T1 cells via single flank implantation and treated with vehicle control and ZE132 (40 mg·kg<sup>-1</sup>, i.p., QD) via i.p. injection after tumour volume reached 30 mm<sup>3</sup> (n = 4 per cohort). (e) ZE132 (mg·kg<sup>-1</sup>) was injected into C57/BL6 mice via i.v. or i.p., and the changes in the drug blood concentration *in vivo* were detected at different time points (n = 4). Results were denoted as means ± SEM, and statistical significance of differences between groups was determined by two-way ANOVA for all tumour growth assays

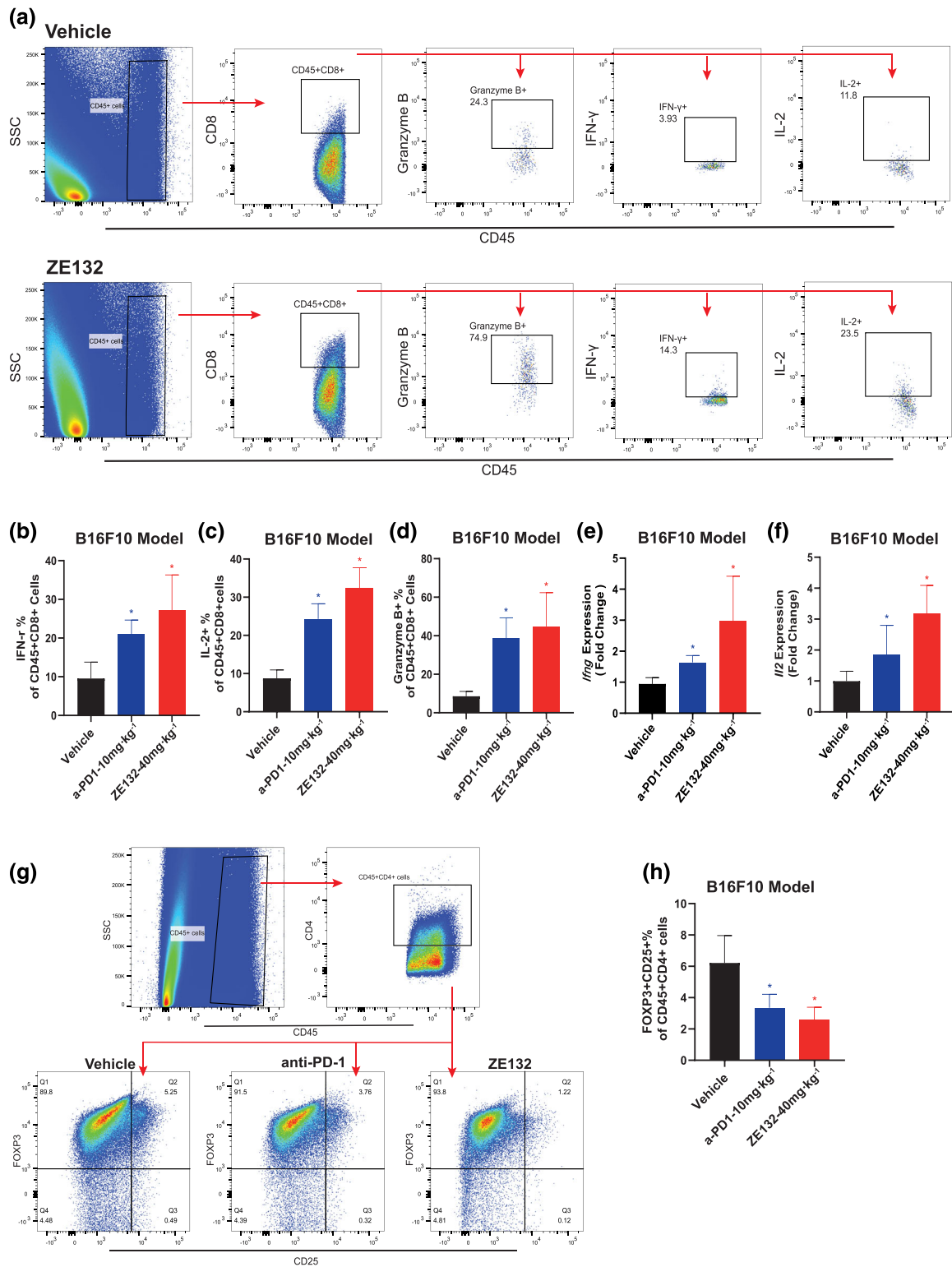


**FIGURE 3** *In vivo* mechanism of action of ZE132. (a) C57BL/6 mice inoculated with B16F10 tumours were treated with a vehicle control, ZE132 (40 mg·kg<sup>-1</sup>, QD) over 10 days. Representative flow panels of cytotoxic T-cells (CTLs) are shown. Gating strategies were also used in other models. (b–d) B16F10 tumours were treated with a vehicle control, ZE132 (40 mg·kg<sup>-1</sup>, QD) and anti-PD-1 (10 mg·kg<sup>-1</sup>, BIW) over 10 days (n = 8 from two batches). Percentages of IFN- $\gamma$ + (b) /IL-2+ (c) /Granzyme B+ (d) cells among the CD45+ CD8+ cell populations in tumours are shown (\**p* < .05). (e, f) qPCR measurement of *Ifng* (e) and *Il2* (f) expression in B16F10 tumours taken from C57BL/6 mice (\**p* < .05). (g) B16F10 tumours were treated with a vehicle control, ZE132 (40 mg·kg<sup>-1</sup>, QD) and anti-PD-1 (10 mg·kg<sup>-1</sup>, BIW) via i.p. injection over 10 days (n = 8 from two batches). Representative flow panels of regulatory T-cells (Tregs) are shown. Gating strategies were used in other models. (h) Percentages of Foxp3+ Tregs in B16F10 tumours are shown (\**p* < .05). Statistical significance of differences between groups was determined by unpaired Student's *t*-test. Results were denoted as means  $\pm$  SEM for experiments performed in triplicate

The above results show that upon blockade of the PD-1/PD-L1 interactions by ZE132, the depletion of T-cells in the TIME is alleviated, increasing cytokines expression increased, tumour suppression enhanced and regulatory T-cells tumour infiltration decreased, leading to robust tumour growth suppression.

#### 4.5 | ZE132 shows a tolerable profile *in vivo*

We investigated the toxic effects of ZE132 *in vivo* to determine its therapeutic window. As shown in previous *in vitro* toxicity tests, ZE132 showed no compound-induced cytotoxicity to cells at  $10 \mu\text{mol}\cdot\text{L}^{-1}$ , whereas ZE132 at  $877 \text{ nmol}\cdot\text{L}^{-1}$  shows 2 folds activity of cytotoxic T-cell compared with vehicle (E:T = 16:1) (Figure 1h). In a mouse maximum lethal dose study, the median lethal dose ( $\text{LD}_{50}$ ) in C57BL/6 mice was  $>400 \text{ mg}\cdot\text{kg}^{-1}$  (supporting information). In the B16F10 (Figure 4a) and CT26 (Figure 4b) efficacy models, the change of body weight in mice in the ZE132-treated group was an  $\sim 2 \text{ g}$  lower ( $\sim 10\%$ ) reduction than in the vehicle group, and the body weight showed a tendency to recover from Days 4 to 8. A similar phenomenon can also be observed in the MC38 model (Figure 4c) and 4T1 model (Figure 4d).

For the *in vivo* toxicity experiments, C57BL/6 mice were divided into three groups according to the administration regimen as follows: vehicle control,  $40 \text{ mg}\cdot\text{kg}^{-1}$  and  $80 \text{ mg}\cdot\text{kg}^{-1}$ , i.p. QD. Treatments lasted for 1 week. The mice were killed and major organs such as the liver, lung, heart, intestine and spleen were processed for histology analysis. The staining results showed that ZE132 does not cause direct toxicity to internal organs at both  $40$  and  $80 \text{ mg}\cdot\text{kg}^{-1}$  (Figure 4e), indicating that ZE132 has good safety and tolerance.

Serum chemistry and haematology studies were performed after a 2-week treatment period, and no differences were found between animals treated with the vehicle control and ZE132 (Figure 4f). This result indicated that ZE132 has no obvious toxicity to mice including no liver toxicity and thus the compound was considered safe.

Overall, we concluded that ZE132 shows a tolerable toxicity profile and a favourable therapeutic window.

#### 4.6 | ZE132 *in vivo* efficacy is related to *Tgfb1* expression level in tumour microenvironments

We found that ZE132 showed different response rates of tumour growth inhibition in B16F10, 4T1, CT26 and MC38 models. Thus, we further investigated the mechanism driving this response. A successful immune reaction requires sufficient cytotoxic T lymphocytes tumour infiltration and a favourable TIME.

Given the strong clinical relevance between dendritic cells (DCs) infiltration and T-cells activation, we next examined whether blockage with ZE132 can functionally modulate DCs in the cancer immunologic microenvironment. Quantitative real-time PCR (qPCR) results showed that *Irfng* mRNA expression levels were increased in the tumour environment.  $\text{IFN}\cdot\gamma$  stimulates the secretion of degeneration factors such

as **CXCL9** by CD103+ DCs, thereby recruiting more cytotoxic T-cells to inhibit tumour growth (Dangaj et al., 2019). As such, we used the gating strategies shown in Figure 5a to identify CXCL9+ CD103+ DCs. CXCL9 secreted from CD103+ DCs is increased in ZE132-treated groups compared with PD-1 antibody-treated group, indicating that ZE132 treatment promotes higher CXCL9 protein expression in B16F10 and CT26 tumour (Figure 5b,c). Similar results were also observed for *Cxcl9* mRNA expression (Figure 5d,e).

CXCL9 plays an important role in the recruitment of CD8+ T-cells (Gorbachev et al., 2007). qPCR was used to detect the *Cd8* mRNA expression in TIME, and the results showed a significant increase in treatment group of B16F10 and CT26 model compared with vehicle group (Figure 5f,g).

Immunohistochemistry staining of CD8 showed that infiltration of CD8+ T-cells is increased in the ZE132 treated tumour compared to that of anti-PD-1 treated tumour (Figure 5h). The positive rate of vehicle cohort was 17%, and positive rate of anti-PD-1 and ZE132 cohort was 25% and 30%, respectively. 4T1 was previously reported as a PD-1 antibody resistance model with an immunosuppressive tumour microenvironment (Meyer et al., 2014; Ostrand-Rosenberg et al., 2020; Pulaski & Ostrand-Rosenberg, 2001). Similar to the PD-1 antibody, ZE132 showed better *in vivo* efficacy in the B16F10 and CT26 models than in the 4T1 model.

qPCR of tumour tissue after treatment demonstrated lower mRNA expression levels of *Tgfb1* in the ZE132-treated cohort, compared to the anti-PD-1 antibody and vehicle cohorts (Figures 5i-k and S4l). This result indicated that ZE132 is more effective in targeting intra-tumour cells compared with the PD-1 antibody and overcomes the immune resistance driven by TGF- $\beta$ .

**Interleukin 10 (IL-10)**, an inhibitory cytokine, is one of the key cytokines negatively impacting immune cell infiltration. qPCR analysis of tumours showed that after treatment of PD-1 antibody and ZE132, *Il10* mRNA expression increased both in B16F10 and CT26 model, whereas the level of *Il10* mRNA expression in ZE132-treated group was lower than that in antibody-treated group (Figure S4m,n). The mRNA expression increases of *Cd274*, *Lag3* and *Havcr2* were observed, but the increase in ZE132-treated group was lower than the PD-1 antibody-treated group (Figure S4o-t). The ZE132 treated group showed a better survival compared with the vehicle group and also demonstrated superior longer survival compared to the anti-PD-1 treated group (Figure S5a,b).

Collectively, these data indicated that ZE132 mediates the blockage of the immune-suppressive TGF- $\beta$  pathway. This may be due to ZE132 being a small molecule, displaying superior tissue permeability compared to antibodies.

#### 4.7 | TGF- $\beta$ expression positively correlated with PD-1/L1 and Tumour mutational burden in cancers

TGF- $\beta$  has been reported to play an important role in cancer development and immunology (Daniele V. F. Tauriello et al., 2018). In an analysis of patients with head and neck squamous cell carcinoma, stomach

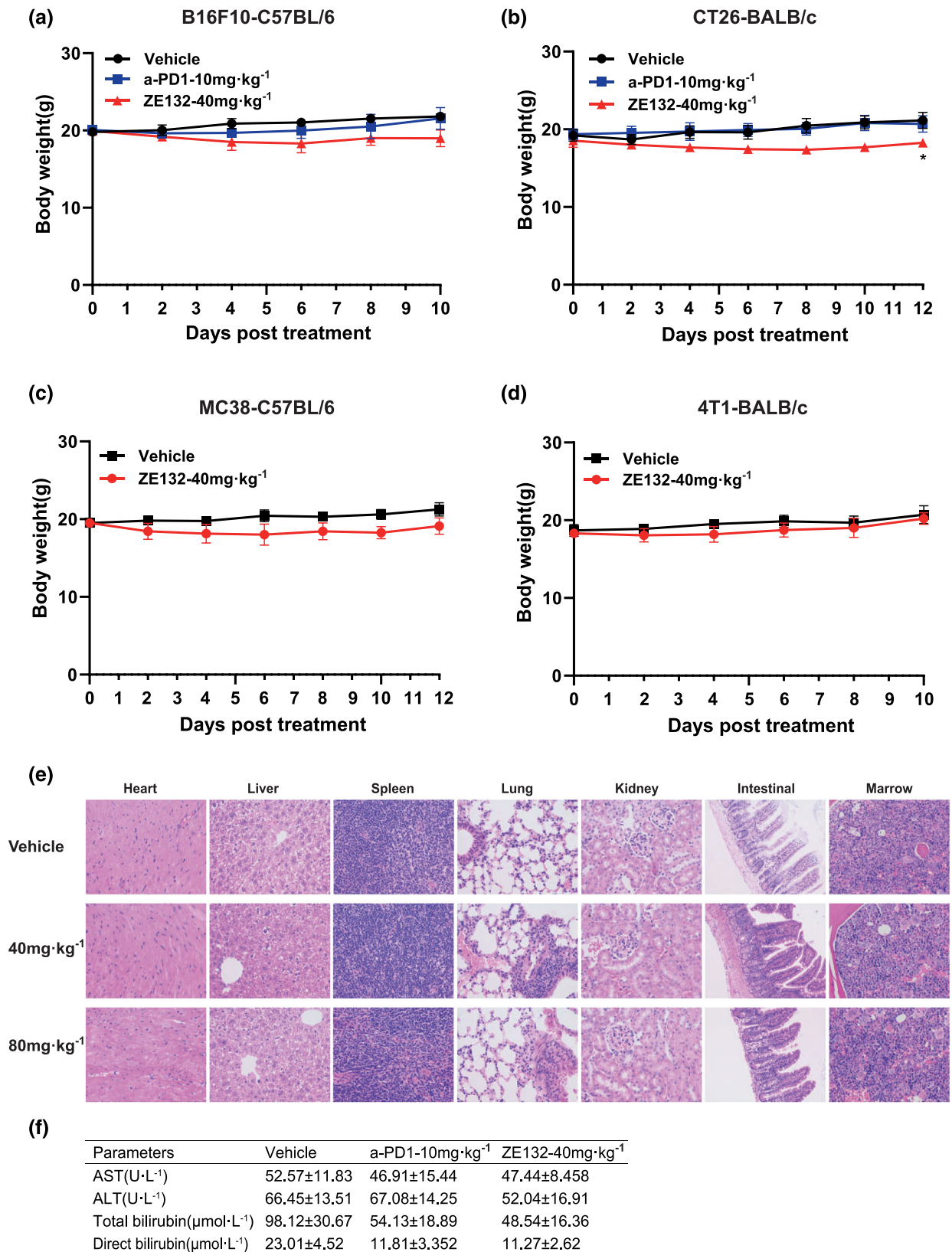


**FIGURE 4** Safety profile of ZE132. (a-d) Body weight changes of (a) B16F10 tumour (n = 5), (b) CT26 tumour (n = 5), (c) MC38 tumour (n = 4), and (d) 4T1 tumour-bearing mice (n = 4) (\**p* < .05). (e) Representative images of H&E staining for organs of C57BL/6 mice treated with vehicle control or ZE132 (40 or 80 mg·kg<sup>-1</sup>) (n = 2). (f) Serum biochemical analysis. After 10 days of treatment, CT26 tumour-bearing mice were killed to obtain blood samples to perform serum biochemical analysis (n = 5). Statistical significance of differences between groups was determined by unpaired Student's *t*-test. Results were denoted as means ± SEM

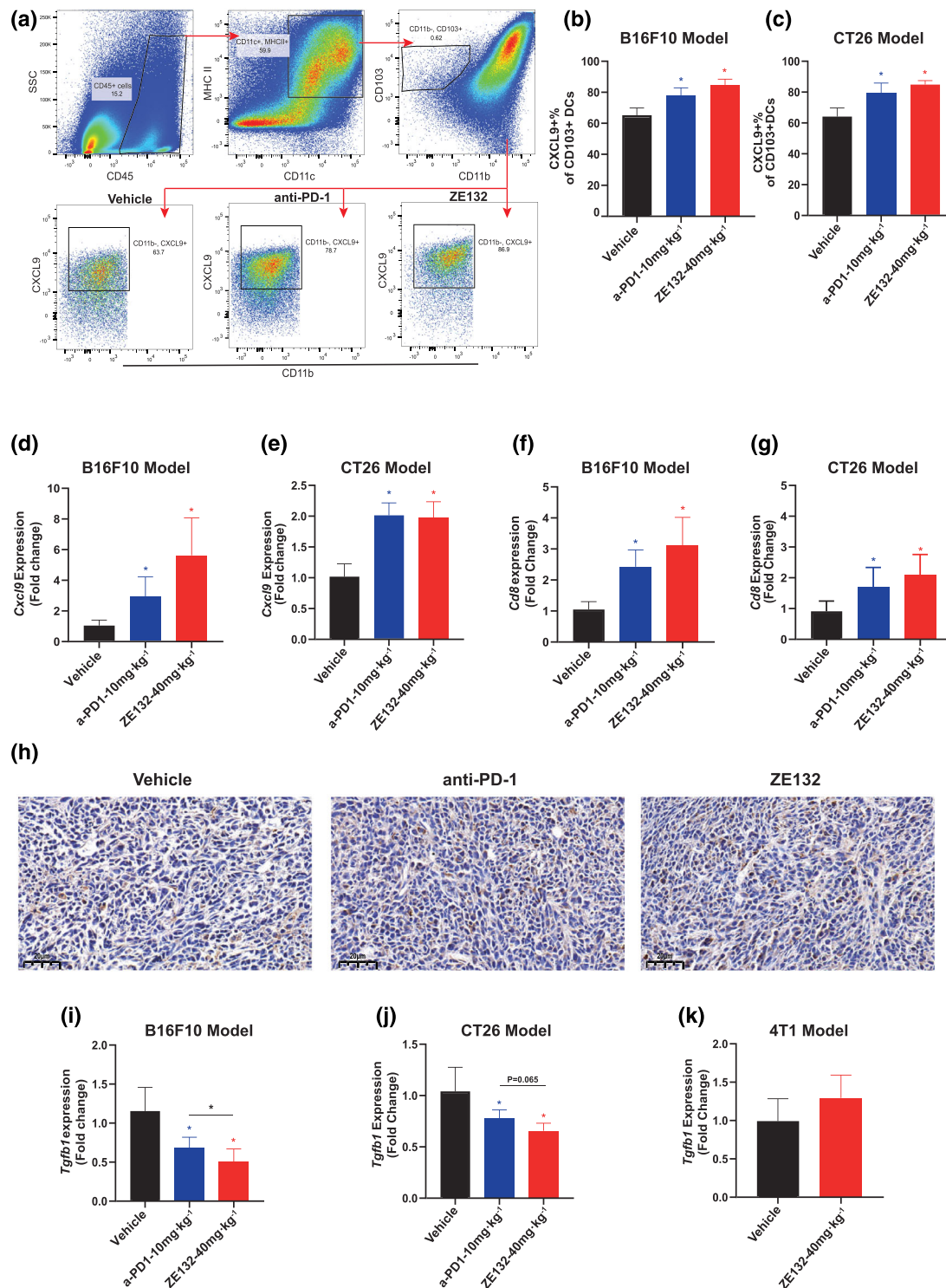


**FIGURE 5** Mechanistic study of ZE132 *in vivo*. (a) C57BL/6 mice inoculated with B16F10 tumours were treated with a vehicle control, ZE132 (40 mg·kg<sup>-1</sup>, QD), and anti-PD-1 (10 mg·kg<sup>-1</sup>, BIW) via i.p. injection for over 10 days. Representative flow panels of CXCL9+ CD103+ DCs are shown. Gating strategies were also used in other models. (b, c) In B16F10 (n = 8 from two batches) (b) and CT26 models (n = 5 per cohort) (c), the percentages of CXCL9+ cells of CD103+ DCs are shown (\**p* < .05). (d, e) qPCR measurement of *Cxcl9* expression in B16F10 tumours (n = 8 from two batches) (d) and CT26 tumours (n = 5 per cohort) (e) (\**p* < .05). (f, g) qPCR measurement of *Cd8* expression in B16F10 tumours (n = 8 from two batches) (f) and CT26 tumours (n = 5 per cohort) (g) (\**p* < .05). (h) After 10 days of treatment, CT26 tumour-bearing mice were killed to obtain tumour samples. Then, the immunohistochemistry assay was used to confirm the upregulated infiltration of CD8+ T-cells in CT26 tumours. (i–k) qPCR measurement of *Tgfb1* expression in B16F10 (n = 8 from two batches) (i), CT26 (n = 5 per cohort) (j), and 4T1 (n = 5 per cohort) (k) tumours (\**p* < .05). Results were denoted as means ± SEM for experiments performed in triplicate, and the statistical significance of differences between groups was determined by unpaired Student's *t*-test

adenocarcinoma, kidney renal clear cell carcinoma and hepatocellular carcinoma, we found that patients with high expression of *TGFB1* had significantly shortened survival, suggesting the TGF- $\beta$ 1 plays an important role in these cancers (Figure S5c–f).

To investigate the correlation between PD-1/PD-L1 and TGF- $\beta$  signalling, we performed analysis in The Cancer Genome Atlas database. As shown in the heatmap, *CD274* and TGF- $\beta$  pathway gene expression was significantly positively correlated in the colon adenocarcinoma (Figure 6a) patient samples. *TGFB1* and *CD274* expression also show the positive correlation in patient samples of colon adenocarcinoma (Figure 6b). The same correlation-ships were also observed in skin cutaneous melanoma (Figure 6c,d) and breast invasive carcinoma (Figure S5g,h) patient samples. *PDCD1* and TGF- $\beta$  pathway gene expression was also significantly positively correlated in the patient samples of breast invasive carcinoma, colon adenocarcinoma and skin cutaneous melanoma patient samples (Figure S6a–f).

Furthermore, we found that TGF- $\beta$  expression was significantly correlated with tumour mutational burden in colon adenocarcinoma from the Cancer Genome Atlas (Figure 6e). Patients with tumour mutational burden may not benefit from immunotherapy. We analysed the association between tumour mutational burden and immunotherapy outcomes using a cohort of colorectal cancer patients treated with immune checkpoint inhibitors. Patients with high tumour mutational burden showed significantly higher overall survival time after immunotherapy than that of patients with low and median tumour mutational burden (Figure 6f). This result indicates that TGF- $\beta$  may be negatively correlated with immune checkpoint inhibitors.

We performed Kaplan–Meier analyses according to the *TGFB1* expression for the other cancer types including breast invasive carcinoma and skin cutaneous melanoma, showing high *TGFB1* expression associated with a good prognosis (Figure S7a,b).

In the data set of before (T0) and after (M1 and M2) treatment of anti-PD-1 for responders, we performed analysis with the RNA-seq data to sort CD8+ T-cell populations according to differential *PDCD1* and *TGFB1* expression patterns. To check the correlation between *PDCD1* and *TGFB1*, we used the two PD-1 positive cell populations, which could possibly lead to selection biases. In both T0 and M1, *PDCD1* show significant positive relationship with *TGFB1* (Figure S7c–g). Our data show that we observed significant positive correlation between *PDCD1* and *TGFB1* gene expression before and after treatment.

In summary, these results indicated that TGF- $\beta$  signalling is positively correlated with PD-1 and PD-L1 in cancers and provided new insights linking TGF- $\beta$  to the outcome of targeting PD-1/PD-L1 in cancers.

## 5 | DISCUSSION

Small-molecule PD-1/PD-L1 inhibitors may have unique pharmacodynamic and pharmacokinetic characteristics, but it is still challenging for designing small molecules because of the hydrophobic, flat, extended interface between PD-1 and PD-L1 without a deep binding pocket

(Zak et al., 2015). Our study identified a potent and selective lead compound (ZE132) that inhibits PD-1/PD-L1 interaction. ZE132 effectively suppresses tumour growth in multiple animal models and exhibits favourable pharmacokinetic features and low toxicity in major organs. ZE132 can overcome tumour resistance to immune checkpoint inhibitors, thus showing robust anti-tumour effects. Our work also elucidated the role of ZE132 in regulating the TIME to favour an immune reaction. We identified the molecular mechanism underlying resistance to ZE132 among the mouse models.

Compared to monoclonal antibodies, ZE132 have significant advantages, including a lower synthesis cost, potential biological activity, good membrane permeability and non-immunogenicity. A shorter half-life period makes treatment more flexible and allows clinicians to administer these molecules intermittently to balance the risk of side effects (Huck et al., 2018). By contrast, monoclonal antibodies are usually polar, heat sensitive and membrane impermeable. Additionally, the clinically approved antibody therapies can target only extracellular molecules (Kaplon & Reichert, 2018). Because ZE132 as a small molecule may have advantage in superior cell permeability compared to antibodies, ZE132 may have a better *in vivo* efficacy and broader response rate in cancer models.

Several series of small-molecule inhibitors of PD-1/PD-L1 interaction have been reported, while biphenyl moiety-containing compounds appeared to be more potent in *in vitro* assay (Wang et al., 2019). However, the in-depth cellular functional evaluations, systemic *in vivo* pharmacological profiling and extensive *in vivo* efficacy studies of these biphenyl-containing compounds remain under-explored. In addition, the taurine moiety significantly improved the potency of hydrophobic biphenyl-containing compounds and such structural design has not been previously reported. Our studies also showed that taurine-containing compounds inhibited PD-1/PD-L1 interaction with higher potency compared to that of BMS-1266. The taurine-containing ZE132 was active in cellular assay. Furthermore, the compound ZD41 showed as good as efficacy of ZE132 in B16F10 model, both of which have the taurine moiety in their structure. Collectively, these data suggested taurine moiety is also beneficial for optimal *in vitro* and cellular potency.

PD-1 binds to one of its two ligands, PD-L1 (also known as B7-H1 and CD274) or PD-L2 (known as B7-DC and CD273), which have close binding affinities (PD-1/PD-L1  $K_d = 10.4 \text{ nmol-L}^{-1}$ , PD-1/PD-L2  $K_d = 11.3 \text{ nmol-L}^{-1}$ ) (Ghioetto et al., 2010). ZE132 shows stronger binding affinity to PD-L1 compared to that of PD-L2.

MC38 has the highest mutational load, then followed by CT26, whereas 4T1 have the lowest mutational load. MC38 had Trp53 heterozygous mutations (G242 V, S258I) and a Smad4 heterozygous mutation (G351R), and these two mutations existed in approximately 12% of human colon cancer. CT26 had homozygous Kras mutations (G12D, V8M). Total CD45+ leukocyte infiltration in syngeneic models is an indicator of cancer immunity and cytolytic activity, which was also highest in CT26 and 4T1 and lowest in B16F10 among the solid tumour models. ZE132 shows significantly improve tumour lymphocyte infiltration in CT26 and B16F10. The poor response in 4T1 model may be due to high heterogeneity of mammary gland tumour of

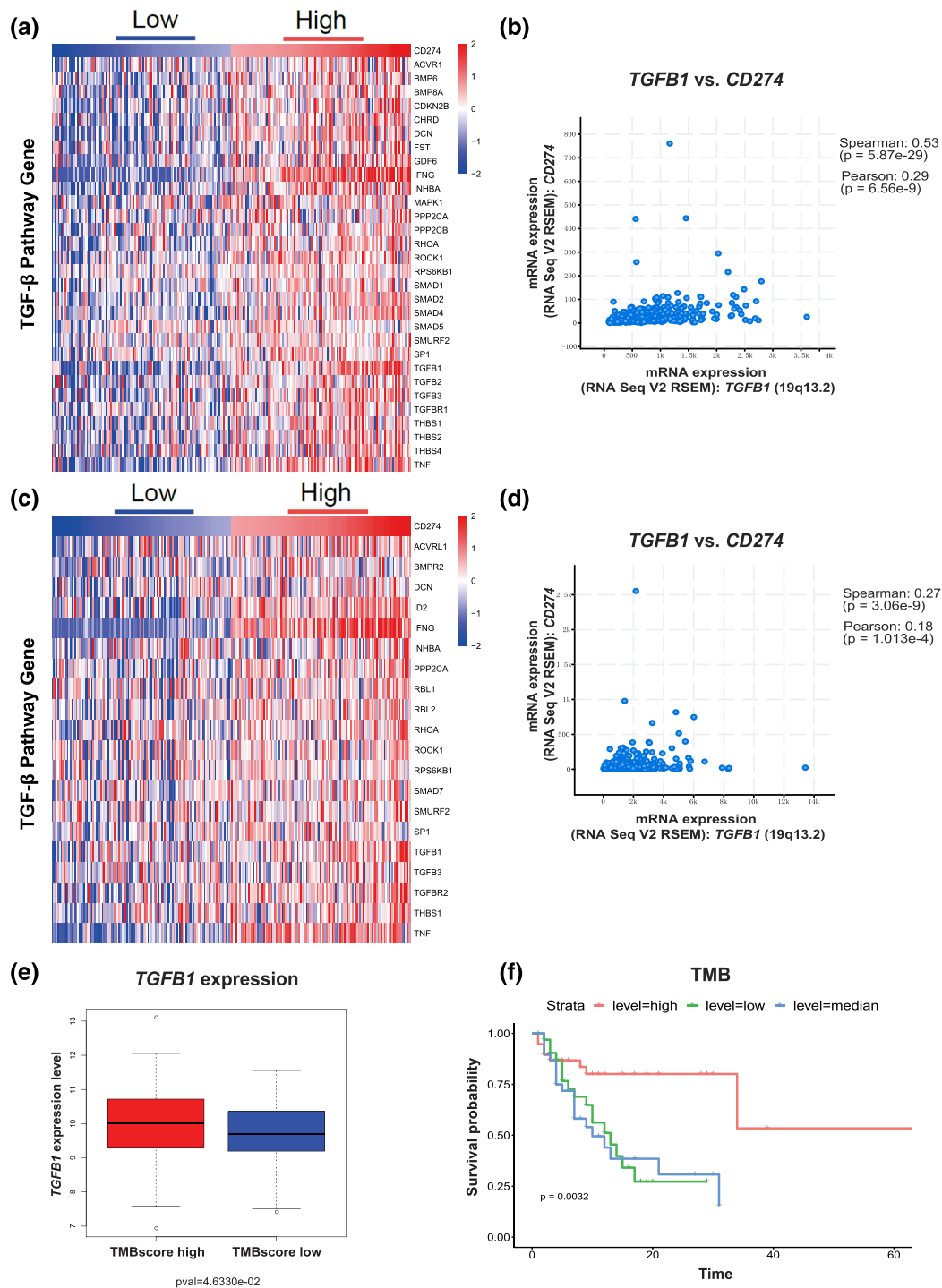


**FIGURE 6** Expression of TGF- $\beta$  is associated with the expression of PD-L1. (a, b) Relative heat map of TGF- $\beta$  pathway gene expression in colon adenocarcinoma (COAD) (a), stratified by CD274 expression level (CD274-hi vs. CD274-lo). High expression is denoted by the top quartile, whereas low infiltration is composed of the bottom quartile of the tumours. Each column represents one sample. Pearson correlation of TGFB1 expression with CD274 expression in the COAD (b) was calculated. (c, d) Relative heat map of TGF- $\beta$  pathway gene expression in skin cutaneous melanoma (c), stratified by CD274 expression level (CD274-hi vs. CD274-lo). High expression is denoted by the top quartile, whereas low infiltration is composed of the bottom quartile of the tumours. Each column represents one sample. Pearson correlation of TGFB1 expression with CD274 expression in the skin cutaneous melanoma (d) was calculated. (e) The Cancer Genome Atlas colon adenocarcinoma (COAD) patient samples were divided into tumour mutational burden high and low groups based on whether their tumour mutational burden scores greater than the median tumour mutational burden score. TGFB1 expression level were shown in boxplot within these tumour mutational burden high and low groups. Two-tail Student's *t*-tests were performed to test the significance of the expression differences within these two groups ( $p$  value  $<.05$ ). (f) Correlation of tumour mutational burden with immunotherapy outcome in colorectal cancer (CRC) specimens.  $p \leq .05$  means statistically significant

mouse. CT26 was highly responsive to CTLA-4 inhibitors, but not to PD-1 inhibitors, whereas B16F10 model did not respond to these checkpoint inhibitors (Zhong et al., 2020). ZE132 shows good efficacy in the high immunogenicity of the CT26 model and low immunogenicity of B16F10 models, suggesting its potential targeting larger patient population.

TGF- $\beta$  is a causative factor of tumour resistance in immune checkpoint therapy (Tauriello et al., 2018). Our findings provide a new approach to improve the inhibition of TGF- $\beta$  signalling via a small-molecule PD-1/PD-L1 inhibitor. Treatment with ZE132 impacts two immunosuppressive pathways (PD-1/L1 immune checkpoints and TGF- $\beta$  signalling), suggesting an approach for dual regulation of the TIME.

TGF- $\beta$  signalling functions as both a tumour suppressor and a tumour promoter (Yang & Moses, 2008). Synergetic inhibition of TGF- $\beta$  signalling and PD-1/PD-L1 checkpoint by small molecules suggests a new approach for dual regulation of the TIME and checkpoint blockade.

TGF- $\beta$  in TIME is associated with cold tumours as well as resistance to treatment of immune checkpoint inhibitors (Ganesh & Masagué, 2018). Existing biomarkers of immune checkpoint inhibitors such as PD-1, PD-L1, microsatellite instability and tumour mutational burden are not sufficient to cover and identify immuno-responsive patients. TGF- $\beta$  is a widespread and profoundly negative molecular hallmark of immunosuppression in many tumour types. Our finding highlights the potential of TGF- $\beta$  as a novel potential biomarker to predict responsiveness to immune checkpoint inhibitors.

Although our studies indicate that ZE132 through targeting PD-1/PD-L1 could be potentially therapeutic for cancer, additional preclinical studies, including but not limited to rat and dog models, are needed to further validate this hypothesis.

In summary, we reported a novel set of small-molecule inhibitors that can effectively block the PD-1/PD-L1 interaction, which not only inhibit checkpoint to active cytotoxic T-cell but also change TIME to reactivate anticancer immunity favouring immune reaction. The lead compound ZE132 shows advantages compared with PD-1 antibody. Given their favourable pharmacological features, minimal toxicity and robust anticancer efficacy, ZE132 serial compounds may be used to treat a wide range of human cancers.

## ACKNOWLEDGEMENTS

National Natural Science Foundation of China (81872895 to D.Z.), Shanghai Science and Technology Commission (18ZR1403900, 20430713600 and 18JC1413800 to D.Z.) National Natural Science Foundation of China (82073682 and 81872724 to Y. Z.), National Science & Technology Major Project “Key New Drug Creation and Manufacturing Program”, China (Grant 2018ZX09711002-004-010 to Y. Z. and 2018ZX09711002-005 to X.L.), Science and Technology Commission of Shanghai Municipality (18431907100 to Y. Z.) and K. C. Wong Education Foundation to Y. Z.

## AUTHOR CONTRIBUTION

C. L. developed the methodology and wrote the manuscript. F. Z., Z.Y. and X.Z. designed and synthesised compounds. L. S., F.H. and

H. W. collected the data. X. L., K. Y., analysed the data and edited the manuscript. Y. Z. and D. Z. designed the experiments, supervised the study and wrote the manuscript.

## CONFLICT OF INTEREST

The authors declare no conflict of interest.

## DECLARATION OF TRANSPARENCY AND SCIENTIFIC RIGOUR

This Declaration acknowledges that this paper adheres to the principles for transparent reporting and scientific rigour of preclinical research as stated in the BJP guidelines for [Design & Analysis](#), [Immunohistochemistry](#) and [Animal Experimentation](#), and as recommended by funding agencies, publishers and other organisations engaged with supporting research.

## DATA AVAILABILITY STATEMENT

Data openly available in a public repository. The data that support the findings of this study are openly available in FigShare (RRID: SCR\_004328) at <https://figshare.com/s/70dc9a28bb2ff43b1823>, reference number DOI: 10.6084/m9.figshare.13270907.

## REFERENCES

- Alexander, S. P. H., Kelly, E., Mathie, A., Peters, J. A., Veale, E. L., Armstrong, J. F., Faccenda, E., Harding, S. D., Pawson, A. J., Sharman, J. L., Southan, C., Buneman, O. P., Cidowski, J. A., Christopoulos, A., Davenport, A. P., Fabbro, D., Spedding, M., Striessnig, J., Davies, J. A., ... Wong, S. S. (2019). The concise guide to pharmacology 2019/20: Introduction and other protein targets. *British Journal of Pharmacology*, 176 Suppl 1(Suppl 1), S1–s20. <https://doi.org/10.1111/bph.14747>
- Bang, Y. J., Doi, T., Kondo, S., Chung, H. C., Muro, K., Dussault, I., Helwig, C., Osada, M., & Kang, Y. K. (2018). 661P—Updated results from a phase I trial of M7824 (MSB0011359C), a bifunctional fusion protein targeting PD-L1 and TGF- $\beta$ , in patients with pretreated recurrent or refractory gastric cancer. *Annals of Oncology*, 29, viii222–viii223. <https://doi.org/10.1093/annonc/mdy282.045>
- Basu, S., Yang, J., Xu, B., Magiera-Mularz, K., Skalniak, L., Musielak, B., Kholodovych, V., Holak, T. A., & Hu, L. (2019). Design, synthesis, evaluation, and structural studies of C(2)-symmetric small molecule inhibitors of programmed cell death-1/programmed death-ligand 1 protein-protein interaction. *Journal of Medicinal Chemistry*, 62(15), 7250–7263. <https://doi.org/10.1021/acs.jmedchem.9b00795>
- Battle, E., & Massagué, J. (2019). Transforming growth factor- $\beta$  signaling in immunity and cancer. *Immunity*, 50(4), 924–940. <https://doi.org/10.1016/j.immuni.2019.03.024>
- Butte, M. J., Keir, M. E., Phamduy, T. B., Sharpe, A. H., & Freeman, G. J. (2007). Programmed death-1 ligand 1 interacts specifically with the B7-1 costimulatory molecule to inhibit T cell responses. *Immunity*, 27(1), 111–122. <https://doi.org/10.1016/j.immuni.2007.05.016>
- Chen, D., Lu, T., Yan, Z., Lu, W., Zhou, F., Lyu, X., Xu, B., Jiang, H., Chen, K., Luo, C., & Zhao, Y. (2019). Discovery, structural insight, and bioactivities of BY27 as a selective inhibitor of the second bromodomains of BET proteins. *European Journal of Medicinal Chemistry*, 182, 111633–111654. <https://doi.org/10.1016/j.ejmech.2019.111633>
- Cheng, B., Ren, Y., Niu, X., Wang, W., Wang, S., Tu, Y., Liu, S., Wang, J., Yang, D., Liao, G., & Chen, J. (2020). Discovery of novel resorcinol dibenzyl ethers targeting the programmed cell death-1/programmed cell death-ligand 1 interaction as potential anticancer agents. *Journal*

- of *Medicinal Chemistry*, 63(15), 8338–8358. <https://doi.org/10.1021/acs.jmedchem.0c00574>
- Curtis, M. J., Alexander, S., Cirino, G., Docherty, J. R., George, C. H., Giembycz, M. A., Hoyer, D., Insel, P. A., Izzo, A. A., Ji, Y., MacEwan, D. J., Sobey, C. G., Stanford, S. C., Teixeira, M. M., Wonnacott, S., & Ahluwalia, A. (2018). Experimental design and analysis and their reporting II: Updated and simplified guidance for authors and peer reviewers. *British Journal of Pharmacology*, 175(7), 987–993. <https://doi.org/10.1111/bph.14153>
- Dangaj, D., Bruand, M., Grimm, A. J., Ronet, C., Barras, D., Duttagupta, P. A., Lanitis, E., Duraiswamy, J., Tanyi, J. L., Benencia, F., Conejo-Garcia, J., Ramay, H. R., Montone, K. T., Powell, D. J., Gimotty, P. A., Facciabene, A., Jackson, D. G., Weber, J. S., Rodig, S. J., ... Coukos, G. (2019). Cooperation between constitutive and inducible chemokines enables T cell engraftment and immune attack in solid tumors. *Cancer Cell*, 35(6), 885–900e810. <https://doi.org/10.1016/j.ccell.2019.05.004>
- Ganesh, K., & Massagué, J. (2018). TGF- $\beta$  inhibition and immunotherapy: Checkmate. *Immunity*, 48(4), 626–628. <https://doi.org/10.1016/j.immuni.2018.03.037>
- Ghiotto, M., Gauthier, L., Serriari, N., Pastor, S., Truneh, A., Nunès, J. A., & Olive, D. (2010). PD-L1 and PD-L2 differ in their molecular mechanisms of interaction with PD-1. *International Immunology*, 22(8), 651–660. <https://doi.org/10.1093/intimm/dxq049>
- Gorbachev, A. V., Kobayashi, H., Kudo, D., Tannenbaum, C. S., Finke, J. H., Shu, S., Farber, J. M., & Fairchild, R. L. (2007). CXC chemokine ligand 9/monokine induced by IFN-gamma production by tumor cells is critical for T cell-mediated suppression of cutaneous tumors. *Journal of Immunology*, 178(4), 2278–2286. <https://doi.org/10.4049/jimmunol.178.4.2278>
- Gropper, Y., Feferman, T., Shalit, T., Salame, T. M., Porat, Z., & Shakhar, G. (2017). Culturing CTLs under hypoxic conditions enhances their cytotoxicity and improves their anti-tumor function. *Cell Reports*, 20(11), 2547–2555. <https://doi.org/10.1016/j.celrep.2017.08.071>
- Guzik, K., Tomala, M., Muszak, D., Konieczny, M., Hec, A., Blaszkiewicz, U., Pustuła, M., Butera, R., Dömling, A., & Holak, T. A. (2019). Development of the inhibitors that target the PD-1/PD-L1 interaction—A brief look at progress on small molecules, peptides and macrocycles. *Molecules*, 24(11), 2071. <https://doi.org/10.3390/molecules24112071>
- Guzik, K., Zak, K. M., Grudnik, P., Magiera, K., Musielak, B., Törner, R., Skalniak, L., Dömling, A., Dubin, G., & Holak, T. A. (2017). Small-molecule inhibitors of the programmed cell death-1/programmed death-ligand 1 (PD-1/PD-L1) interaction via transiently induced protein states and dimerization of PD-L1. *Journal of Medicinal Chemistry*, 60(13), 5857–5867. <https://doi.org/10.1021/acs.jmedchem.7b00293>
- Hu, B., Gilkes, D. M., & Chen, J. (2007). Efficient p53 activation and apoptosis by simultaneous disruption of binding to MDM2 and MDMX. *Cancer Research*, 67(18), 8810–8817. <https://doi.org/10.1158/0008-5472.Can-07-1140>
- Huck, B. R., Kötzner, L., & Urbahns, K. (2018). Small molecules drive big improvements in immuno-oncology therapies. *Angewandte Chemie (International Ed. in English)*, 57(16), 4412–4428. <https://doi.org/10.1002/anie.201707816>
- Hui, E., Cheung, J., Zhu, J., Su, X., Taylor, M. J., Wallweber, H. A., Sasmal, D. K., Huang, J., Kim, J. M., Mellman, I., & Vale, R. D. (2017). T cell costimulatory receptor CD28 is a primary target for PD-1-mediated inhibition. *Science*, 355(6332), 1428–1433. <https://doi.org/10.1126/science.aaf1292>
- Hwang, S. J., Carlos, G., Chou, S., Wakade, D., Carlino, M. S., & Fernandez-Penas, P. (2016). Bullous pemphigoid, an autoantibody-mediated disease, is a novel immune-related adverse event in patients treated with anti-programmed cell death 1 antibodies. *Melanoma Research*, 26(4), 413–416. <https://doi.org/10.1097/cmr.0000000000000260>
- Kaplon, H., & Reichert, J. M. (2018). Antibodies to watch in 2018. *MAbs*, 10(2), 183–203. <https://doi.org/10.1080/19420862.2018.1415671>
- Kawamoto, S. A., Thompson, A. D., Coleska, A., Nikolovska-Coleska, Z., Yi, H., & Wang, S. (2009). Analysis of the interaction of BCL9 with  $\beta$ -catenin and development of fluorescence polarization and surface plasmon resonance binding assays for this interaction. *Biochemistry*, 48(40), 9534–9541. <https://doi.org/10.1021/bi900770z>
- Konieczny, M., Musielak, B., Kocik, J., Skalniak, L., Sala, D., Czub, M., Magiera-Mularz, K., Rodriguez, I., Myrcha, M., Stec, M., Siedlar, M., Holak, T. A., & Plewka, J. (2020). Di-bromo-based small-molecule inhibitors of the PD-1/PD-L1 immune checkpoint. *Journal of Medicinal Chemistry*, 63(19), 11271–11285. <https://doi.org/10.1021/acs.jmedchem.0c01260>
- Lilley, E., Stanford, S. C., Kendall, D. E., Alexander, S. P. H., Cirino, G., Docherty, J. R., George, C. H., Insel, P. A., Izzo, A. A., Ji, Y., Panettieri, R. A., Sobey, C. G., Stefanska, B., Stephens, G., Teixeira, M., & Ahluwalia, A. (2020). ARRIVE 2.0 and the British Journal of Pharmacology: Updated guidance for 2020. *British Journal of Pharmacology*, 177(16), 3611–3616. <https://doi.org/10.1111/bph.15178>
- Meyer, C., Cagnon, L., Costa-Nunes, C. M., Baumgaertner, P., Montandon, N., Leyvraz, L., Michielin, O., Romano, E., & Speiser, D. E. (2014). Frequencies of circulating MDSC correlate with clinical outcome of melanoma patients treated with ipilimumab. *Cancer Immunology, Immunotherapy*, 63(3), 247–257. <https://doi.org/10.1007/s00262-013-1508-5>
- Miller, M. M., Mapelli, C., Allen, M. P., Bowsher, M. S., Gillis, E. P., Langley, D. R., Mull, E., Poirier, M. A., Sanghvi, N., Sun, L. Q., Tenney, D. J., Yeung, K. S., Zhu, J. L., Gillman, K. W., Zhao, Q., Grant-Young, K. A., Scola, P. M., & Cornelius, L. A. M. (2014). Macrocyclic inhibitors of the PD-1/PD-L1 and CD80(B7-H1)/PD-L1 protein/protein interactions. In *Bristol-Myers Squibb company*.
- Naidoo, J., Page, D. B., Li, B. T., Connell, L. C., Schindler, K., Lacouture, M. E., Postow, M. A., & Wolchok, J. D. (2015). Toxicities of the anti-PD-1 and anti-PD-L1 immune checkpoint antibodies. *Annals of Oncology*, 26(12), 2375–2391. <https://doi.org/10.1093/annonc/mdv383>
- Ostrand-Rosenberg, S., Beury, D. W., Parker, K. H., & Horn, L. A. (2020). Survival of the fittest: How myeloid-derived suppressor cells survive in the inhospitable tumor microenvironment. *Cancer Immunology, Immunotherapy*, 69(2), 215–221. <https://doi.org/10.1007/s00262-019-02388-8>
- Patsoukis, N., Brown, J., Petkova, V., Liu, F., Li, L., & Boussiotis, V. A. (2012). Selective effects of PD-1 on Akt and Ras pathways regulate molecular components of the cell cycle and inhibit T cell proliferation. *Science Signaling*, 5(230), ra46. <https://doi.org/10.1126/scisignal.2002796>
- Percie du Sert, N., Hurst, V., Ahluwalia, A., Alam, S., Avey, M. T., Baker, M., Browne, W. J., Clark, A., Cuthill, I. C., Dirnagl, U., Emerson, M., Garner, P., Holgate, S. T., Howells, D. W., Karp, N. A., Lazic, S. E., Lidster, K., MacCallum, C. J., Macleod, M., ... Würbel, H. (2020). The ARRIVE guidelines 2.0: Updated guidelines for reporting animal research. *PLoS Biology*, 18(7), e3000410. <https://doi.org/10.1371/journal.pbio.3000410>
- Perez, H. L., Cardarelli, P. M., Deshpande, S., Gangwar, S., Schroeder, G. M., Vite, G. D., & Borzilleri, R. M. (2014). Antibody-drug conjugates: Current status and future directions. *Drug Discovery Today*, 19(7), 869–881. <https://doi.org/10.1016/j.drudis.2013.11.004>
- Postow, M. A. (2015). Managing immune checkpoint-blocking antibody side effects. *American Society of Clinical Oncology Educational Book*, 76–83. [https://doi.org/10.14694/EdBook\\_AM.2015.35.76](https://doi.org/10.14694/EdBook_AM.2015.35.76)
- Pulaski, B. A., & Ostrand-Rosenberg, S. (2001). Mouse 4T1 breast tumor model. *Current Protocols in Immunology, Chapter 20*, Unit 20.22. doi: <https://doi.org/10.1002/0471142735.im2002s39>
- Qin, M., Cao, Q., Zheng, S., Tian, Y., Zhang, H., Xie, J., Xie, H., Liu, Y., Zhao, Y., & Gong, P. (2019). Discovery of [1,2,4]triazolo[4,3-*a*]pyridines as potent inhibitors targeting the programmed cell death-1/programmed cell death-ligand 1 interaction. *Journal of Medicinal*

- Chemistry*, 62(9), 4703–4715. <https://doi.org/10.1021/acs.jmedchem.9b00312>
- Sasikumar, P. G., Ramachandra, M., Vadlamani, S., Shrimali, K., & Subbarao, K. (2012). Therapeutic compounds for immunomodulation. In *Aurigene Discovery Technologies Limited*.
- Sasikumar, P. G., Ramachandra, M., Vadlamani, S. K., Vemula, K. R., Satyam, L. K., Subbarao, K., Shrimali, R. K., & Kandepu, S. (2011). Immunosuppression modulating compounds. In *Aurigene discovery technologies limited*.
- Sasikumar, P. G., Ramachandra, R. K., Adurthi, S., Dhudashiya, A. A., Vadlamani, S., Vemula, K., Vunnum, S., Satyam, L. K., Samiulla, D. S., Subbarao, K., Nair, R., Shrimali, R., Gowda, N., & Ramachandra, M. (2019). A rationally designed peptide antagonist of the PD-1 signaling pathway as an immunomodulatory agent for cancer therapy. *Molecular Cancer Therapeutics*, 18(6), 1081–1091. <https://doi.org/10.1158/1535-7163.Mct-18-0737>
- Sharpe, A. H., Butte, M. J., & Oyama, S. (2011). Modulators of immunoinhibitory receptor PD-1, and methods of use thereof. In *President and fellows of Harvard College*.
- Sharpe, A. H., & Pauken, K. E. (2018). The diverse functions of the PD1 inhibitory pathway. *Nature Reviews. Immunology*, 18(3), 153–167. <https://doi.org/10.1038/nri.2017.108>
- Sun, J. Y., Zhang, D., Wu, S., Xu, M., Zhou, X., Lu, X. J., & Ji, J. (2020). Resistance to PD-1/PD-L1 blockade cancer immunotherapy: Mechanisms, predictive factors, and future perspectives. *Biomarker Research*, 8, 35–45. <https://doi.org/10.1186/s40364-020-00212-5>
- Tauriello, D. V. F., Palomo-Ponce, S., Stork, D., Berenguer-Llergo, A., Badia-Ramentol, J., Iglesias, M., Sevillano, M., Ibiza, S., Cañellas, A., Hernando-Momblona, X., Byrom, D., Matarin, J. A., Calon, A., Rivas, E. I., Nebreda, A. R., Riera, A., Attolini, C. S. O., & Batlle, E. (2018). TGF $\beta$  drives immune evasion in genetically reconstituted colon cancer metastasis. *Nature*, 554(7693), 538–543. <https://doi.org/10.1038/nature25492>
- Taylor, A., Harker, J. A., Chanthong, K., Stevenson, P. G., Zuniga, E. I., & Rudd, C. E. (2016). Glycogen synthase kinase 3 inactivation drives Tbet-mediated downregulation of co-receptor PD-1 to enhance CD8(+) cytolytic T cell responses. *Immunity*, 44(2), 274–286. <https://doi.org/10.1016/j.immuni.2016.01.018>
- Topalian, S. L., Drake, C. G., & Pardoll, D. M. (2015). Immune checkpoint blockade: A common denominator approach to cancer therapy. *Cancer Cell*, 27(4), 450–461. <https://doi.org/10.1016/j.ccell.2015.03.001>
- Wang, T., Wu, X., Guo, C., Zhang, K., Xu, J., Li, Z., & Jiang, S. (2019). Development of inhibitors of the programmed cell death-1/programmed cell death-ligand 1 signaling pathway. *Journal of Medicinal Chemistry*, 62(4), 1715–1730. <https://doi.org/10.1021/acs.jmedchem.8b00990>
- Yang, L., & Moses, H. L. (2008). Transforming growth factor beta: Tumor suppressor or promoter? Are host immune cells the answer? *Cancer Research*, 68(22), 9107–9111. <https://doi.org/10.1158/0008-5472.Can-08-2556>
- Yarchoan, M., Hopkins, A., & Jaffee, E. M. (2017). Tumor mutational burden and response rate to PD-1 inhibition. *The New England Journal of Medicine*, 377(25), 2500–2501. <https://doi.org/10.1056/NEJMc1713444>
- Zak, K. M., Kitel, R., Przetocka, S., Golik, P., Guzik, K., Musielak, B., Dömling, A., Dubin, G., & Holak, T. A. (2015). Structure of the complex of human programmed death 1, PD-1, and its ligand PD-L1. *Structure*, 23(12), 2341–2348. <https://doi.org/10.1016/j.str.2015.09.010>
- Zhong, W., Myers, J. S., Wang, F., Wang, K., Lucas, J., Rosfjord, E., Lucas, J., Hooper, A. T., Yang, S., Lemon, L. A., Guffroy, M., May, C., Bienkowska, J. R., & Rejto, P. A. (2020). Comparison of the molecular and cellular phenotypes of common mouse syngeneic models with human tumors. *BMC Genomics*, 21(1), 2–19. <https://doi.org/10.1186/s12864-019-6344-3>
- Zhou, H., Chen, J., Meagher, J. L., Yang, C.-Y., Aguilar, A., Liu, L., Bai, L., Cong, X., Cai, Q., Fang, X., Stuckey, J. A., & Wang, S. (2012). Design of Bcl-2 and Bcl-xL inhibitors with subnanomolar binding affinities based upon a new scaffold. *Journal of Medicinal Chemistry*, 55(10), 4664–4682. <https://doi.org/10.1021/jm300178u>
- Zou, W., Wolchok, J. D., & Chen, L. (2016). PD-L1 (B7-H1) and PD-1 pathway blockade for cancer therapy: Mechanisms, response biomarkers, and combinations. *Science Translational Medicine*, 8(328), 328rv324. <https://doi.org/10.1126/scitranslmed.aad7118>

## SUPPORTING INFORMATION

Additional supporting information may be found online in the Supporting Information section at the end of this article.

**How to cite this article:** Liu, C., Zhou, F., Yan, Z., Shen, L., Zhang, X., He, F., Wang, H., Lu, X., Yu, K., Zhao, Y., & Zhu, D. (2021). Discovery of a novel, potent and selective small-molecule inhibitor of PD-1/PD-L1 interaction with robust *in vivo* anti-tumour efficacy. *British Journal of Pharmacology*, 1–20. <https://doi.org/10.1111/bph.15457>